Lagrangian Overturning and the Madden Julian Oscillation

by Patrick Haertel [1], Katherine Straub [2], Alexey Fedorov [1]

[1] Yale University, New Haven, Connecticut, United States

[2] Susquehanna University, Selinsgrove, Pennsylvania, United States

Submitted to Quarterly Journal of the Royal Meteorological Society, 12 October 2012

Corresponding author address: Dr. Patrick Haertel, Geology and Geophysics, Yale University, 210 Whitney Ave, New Haven, CT 06510, USA E-mail: patrick.haertel@yale.edu.

ABSTRACT

The Madden Julian Oscillation (MJO), a planetary scale disturbance in zonal winds and equatorial convection that dominates intraseasonal variability in the tropics, is a challenge to explain and notoriously difficult to simulate with conventional climate models. This study discusses numerical experiments conducted with a novel Lagrangian atmospheric model (LAM) that produces surprisingly robust and realistic MJOs, even at very low resolution. The LAM represents an atmosphere as a collection of conforming air parcels whose motions are predicted using Newtonian mechanics. The model employs a unique convective parameterization, referred to as Lagrangian Overturning (LO), in which overlapping air parcels exchange vertical positions in convectively unstable regions. A key model parameter for simulating MJOs is the vertical position swap frequency, with the most frequent and strongest MJOs occuring when LO is applied many times per model time step, which equates to having rapid convective updrafts and downdrafts. Idealized experiments aimed at identifying the most fundamental dynamics of the LAM MJO suggest that convective entrainment/detrainment and the Coriolis force are necessary for simulating MJOs using the LAM, and that surface friction, wind-dependent surface fluxes, and parameterized convective momentum transport are not necessary, but affect MJO structure, intensity, and propagation speed. While the LAM can simulate MJOs with a constant radiative cooling, MJO intensity and structure are more realistic when radiative cooling depends on longwave optical depth and temperature. An important conclusion of this paper is that the most fundamental dynamics of the MJO are captured by the LO convective parameterization coupled with planetary scale equatorial wave dynamics.

1. Introduction

The Madden Julian Oscillation (MJO) is a planetary scale 30-60 day variation in zonal winds and moist convection that occurs near the equator (Madden and Julian 1971, 1972; Madden and Julian 1995; Zhang 2005). The region of active convection in the MJO typically propagates slowly eastward (~5 $m\ s^{-1}$; Weickman et al. 1985) starting over the western Indian Ocean and diminishing just east of the International Date Line, and it includes smaller scale, higher frequency disturbances moving both eastward and westward (Nakazawa 1998; Hendon and Liebman 1994). An approaching MJO convective disturbance is preceded by easterly wind perturbations in the lower troposphere and westerly perturbations in the upper troposphere, as well as a gradual moistening of the lower troposphere that deepens with deepening convection; wind perturbations then reverse and the troposphere dries out following the passage of the convective center (Kiladis et al. 2005). There have been many theories put forward to explain the genesis, propagation, and structure of the MJO (e.g., see review by Wang 2005), including radiative destabilization (Raymond 2001), wind-induced surface heat exchange (Emanuel 1987), the discharge-recharge hypothesis (Blade and Hartmann 1993), wave-CISK (Lau and Peng 1987), coupling with equatorial Rossby waves (Majda and Stechmann 2009), and the characterizatrion of the MJO as a moisture mode (e.g. Sobel and Maloney 2012), but there is not yet a scientific consensus on what constitutes the most fundamental dynamics of the MJO.

Conventional climate models continue to struggle to properly represent the MJO, with inaccuracies in precipitation amplitude, eastward propagation, and period (e.g., Lin et al. 2006; Kim et al. 2009; Kim et al. 2011). This deficiency of climate models is particularly troubling because the MJO has been shown to have global effects on weather and climate, impacting the El Nino Southern Oscillation (e.g., Kessler and Kleeman 2000, Kessler 2001, Fedorov, 2002, Federov et al. 2003), tropical cyclone formation (Maloney and Hartmann 2000; Barrett and Leslie 2009), Asian and North American monsoons (Wu et al. 1999; Lorenz and Hartmann 2006), and even high-latitude weather (Vecchi and Bond 2003; Cassou 2008). While there are many possible causes for poor simulations of MJOs, recent success in simulating MJOs with the

cloud-resolving or "super" convective parameterization (e.g., Grabowski 2001, Khairoutdinow et al. 2001; Thayer-Calder and Randall 2009) suggest that conventional cumulus parameterizations might lack physics fundamental to the MJO.

In this study it is shown that a Lagrangian framework for fluid modeling and convective parameterization has advantages for simulating MJOs. A recently developed Lagrangian atmospheric model (LAM; Haertel and Straub 2010) is used to simulate circulations on an aquaplanet, with domains ranging from tropical channel to near global. The model employs a unique convective parameterization, referred to as Lagrangian Overturning (LO), in which overlapping air parcels exchange vertical positions in convectively unstable regions. When the LO parameterization is tuned to observations and realistic SSTs are prescribed, robust MJOs spontaneously form and have realistic structure, propagation, and locations of formation and dissipation. Physics reduction experiments reveal the most fundamental dynamics of the MJOs simulated with the LAM, and the sensitivity of MJO structure to radiative forcing is explored.

This study is organized as follows. Section 2 describes the LAM. Section 3 presents simulations of MJOs conducted with an idealized tropical channel version of the LAM. In Section 4 a larger modeling domain is used, and MJOs are simulated with observed SST patterns. Section 5 examines how MJO amplitude and structure depend on the radiation scheme. Section 6 discusses the relationship between MJO activity and basic state winds and precipitation patterns. Section 7 is a summary and discussion.

2. Lagrangian Atmospheric Model

The LAM represents an atmosphere as a collection of conforming air parcels whose motions are predicted using Newtonian mechanics. It was created by modifying a Lagrangian ocean model also based on the conforming parcel concept (Fig. 1; Haertel and Randall 2002; Haertel et al. 2004; Haertel et al. 2009; Van Roekel et al. 2009; Haertel and Fedorov 2012). Details on the construction of the LAM are provided by Haertel and Straub (2010); this section

reviews the model equations and column physics, and describes several new model features.

2.1 Equations of Motion

The LAM simulates fluid behavior by predicting motions of individual air parcels using classical physics. The equations of motion for an individual parcel are as follows:

$$\frac{d\mathbf{x}}{dt} = \mathbf{v} \tag{1}$$

$$\frac{d\mathbf{v}}{dt} + f\ \mathbf{k} \times \mathbf{v} = \mathbf{A}_p + \mathbf{A}_m \tag{2}$$

where $\mathbf{x}$ is horizontal position, t is time, $\mathbf{v}$ is horizontal velocity, f is the Coriolis parameter, $\mathbf{k}$ is the unit vector in the vertical, $\mathbf{A}_p$ is the horizontal acceleration of the parcel resulting from pressure, and $\mathbf{A}_m$ is the horizontal acceleration from parameterized turbulent mixing of momentum. The pressure acceleration $\mathbf{A}_p$ results form the net force of pressure integrated over the surface of the parcel and includes contributions from other parcels and bottom topography (Haertel and Straub 2010). The turbulent drag $\mathbf{A}_m$ is implemented by allowing parcels to exchange momentum with their nearest neighbors (e.g. Haertel et al. 2004; Haertel et al. 2009). Parcels' horizontal positions and accelerations are explicity predicted, but vertical positions are implicitly determined by the parcel stacking order (Haertel and Randall 2002). For example, a parcel ascends when it rides up and over a ridge in bottom topography or other parcels, or when parcels converge beneath it.

2.2 LO Convective Parameterization and other Column Physics

The LAM includes a unique convective parameterization (LO) in which overlapping parcels in convectively unstable regions exchange vertical positions (Fig. 2). It is applied to one column of parcels at a time beginning with the lowest pair of parcels. A test is performed to see if swapping parcel vertical positions (or the pressure of their centers) leads to a higher potential

temperature for the rising parcel, in which case the vertical swap is performed. The physical processes LO is intended to represent are 1) the upward motion in convective clouds and 2) the subsidence around them (Fig. 2). In practice, the majority of the parcels in a column descend slowly while a few parcels ascend rapidly, which is consistent with air parcel behavior in nature in convecting regions. However, some parcels in convecting regions also descend more rapidly owing to effects of evaporative cooling as in convective and stratiform downdrafts (Haertel and Straub 2010). While the parcel swapping mimics atmospheric convection, the horizontal size of parcels in the model is typically much greater than that of convective cells in nature, so that a rising parcel in the model represents the collective effects of many updrafts in nature.

There are only three adjustable parameters within the LO scheme as it is currently implemented in the LAM: the width of the columns, the frequency of vertical position swaps, and the mixing between ascending and descending parcels. Since each parcel maintains a constant amount of mass throughout a simulation, the mixing is an exchange of equal amounts of mass between two parcels and represents both entrainment and detrainment. It turns out that MJO behavior is strongly sensitive to the swap frequency, with intense and frequent MJOs occuring with high swap freqencies (Section 3.2). Using wide columns and a high level of mixing also enhances MJO activity.

Additional column physics implemented in the LAM by Haertel and Straub (2010) include: 1) a prescribed constant radiative cooling in the troposphere (˜ 1 K/day) with a restoring of stratospheric temperatures to observed values; 2) a constant evaporation rate for falling rain; and 3) surface fluxes of latent heat, sensible heat, and momentum that have the form $F = C\Delta$ where C is a turbulent exchange coefficient and Δ denotes a difference between variables across the water-air interface (e.g., specific humidity, potential temperature). Most of the column physics are tuned using data from the Coupled Ocean Atmosphere Response Experiment Intensive Flux Array (COARE IFA; Ciesielski et al. 2003), which were collected over the western Pacific warm pool during a period when the MJO was active (e.g., Lin and Johnson 1996). The LO mixing parameter (entrainment/detrainment) and the evaporation parameter are

selected so that simulated profiles of temperature and humidity in convecting regions in the deep tropics are close to those observed over the COARE IFA (e.g., Fig. 3).

2.3 New Model Features

The version of the LAM used for the idealized model runs presented in Sections 3 and 4 includes several new features: 1) a modified leapfrog time differencing that replaces third-order Adams-Bashforth time differencing and allows a longer time step (i.e. greater computational efficiency); 2) a Mercator projection in place of the spherical geometry described by Haertel et al. (2004), which is more numerically stable with the new time differencing and also more computationally efficient; and 3) wind-dependent surface fluxes, with turbulent exchange coefficients for latent and sensible heat fit to data collected within the COARE IFA. For the more realistic simulations presented in Sections 5 and 6, the LAM also uses a new radiation scheme based on that of Frierson et al. (2006) (described in Section 5), and includes a prognostic variable for cloud water, which is converted to rainwater when mixing ratios exceed 1 $g\ kg^{-1}$.

3. Tropical Channel Simulations

This section discusses a series of LAM simulations conducted with an idealized tropical channel model with a prescribed zonally symmetric sea surface temperature. The purpose of these simulations is to determine how the organization of convection changes with variations in parameters for the LO convective scheme, and in particular, which parameter regimes yield MJOs. Physics reduction experiments are also conducted with the goal of identifying the most fundamental dynamics of MJOs simulated with the LAM.

3.1 Model Configuration

For all of the simulations presented in this section a prescribed zonally symmetric sea surface temperature (SST) is used (Fig. 4) based on the control case of Neale and Hoskins (2000), but with a maximum SST equal to the average SST during the COARE Intensive

Operation Period (Webster and Lucas 1992). This modification was made to faciliate comparisons between simulated profiles of moisture and temperature with those observed over the COARE IFA (e.g., Fig. 3). The model uses rather large air parcels whose radii are 12 degrees in latitude and 30 degrees in longitude, and which have a maximum vertical thickness of about 10 hPa. However, the reader is cautioned not to equate the parcel size with an equivalent resolution in an Eulerian model. In most respects (other than in calculating the pressure force) the parcels are treated as points of mass, and it has been our experience that the equivalent horizontal resolution in Eulerian models is 1-3 times lower than the parcel radius, and the equivalent vertical resolution is 1-9 times higher than the maximum parcel vertical thickness. In other words, a layer several parcels thick with staggered parcel centers tends to behave like a single layer in an Eulerian model. Moreover, as shown by Haertel (2012) and in the appendix, MJO structure is not strongly sensitive to increases in resolution. The tropical channel model domain has a width of 360 degrees in longitude, and a meridional span of 60^o in latitude near the surface (30 S to 30 N), but which increases with height owing to sloping meridional boundaries.

3.2 Idealized MJO Simulations

Convectively coupled Kelvin waves were ubiquitious in initial experiments conducted with the LAM tropical aquaplanet model, and in some cases there were also relatively weak MJOs (Haertel and Straub 2010). However, we recently more thoroughly explored the parameter space for the LO convective scheme, and found that one key to generating strong MJOs is sub-cycling the vertical position swap of parcels many times per dynamics time step. Figure 5 shows time-longitude series of rainfall for several simulations that make use of the COARE-tuned parameters listed in Table 1, but vary the LO vertical position swap frequency (i.e. the number of times LO is subcycled per model time step). With a swap frequency (SF) of 1, the prevailing convective organization is convectively coupled Kelvin waves with a wave number 2 pattern that propagate eastward at 20-25 $m\ s^{-1}$ (Fig 5a). When the SF is increased to 3 there are slower, lower frequency envelopes of convection with more intense rainfall in addition to the Kelvin waves

(Fig 5b). When SF is further increased to 7 and then 12, these large slow disturbances becomer stronger and long-lived, and circle the globe (Fig. 5c-d). We tried several values for SF greater than 12 and found that there was little further change to convective organization.

A physical interpretation of the SF parameter is that it relates to the velocity of convective updrafts and downdrafts, and also the rate at which parameterized convection removes convective instability. In nature, an air parcel's bouyancy determines vertical accelerations, and in the future we plan to use parcel buoyancies to constrain SF in the LAM. However, at the present time SF is a prescribed model parameter that is tuned to produce as realistic a convective organization as possible. The reason(s) why MJO behavior is so sensitive SF are not fully understood. Several possibilities include: 1) a low value of SF equates to excessive most convective damping (Emanuel et al. 1994); 2) the higher the value of SF the more rapidly moisture can be exported from the surface boundary layer; 3) momentum transport by vertically displaced parcels is more significant for higher values of SF.

Based on careful analyses of the horizontal and vertical structures of the long-lived disturbances like those shown in Figs. 5c-d (which are presented in detail for simulations with realistic prescribed SSTs in Sections 4-5), we have identified them as MJOs. For example, the idealized MJO shown in Fig. 5d exhibits several key differences from convectively coupled Kelvin waves simulated with the LAM; not only is the MJO envelope much slower and larger, but it also has a first baroclinic wind structure (Fig. 6), with deep low-level easterly and upper-level westerly perturbations ahead of the convective center, and opposite wind perturbations following the convective center. In contrast, convectively coupled Kelvin waves simulated with the LAM have a second baroclinic wind structure (Haertel and Straub 2010), with maxima in perturbations at the surface, at midlevels, and in the upper troposphere as is found in observations of Kelvin waves (Straub and Kiladis 2003).

3.3 Physics Reduction Experiments

The following experiments help to identify the most fundamental dynamics of the idealized MJOs simulated with the LAM in the tropical aquaplanet configuration. In each case the model is run with MJO-favorable parameters (an SF of 12 with other parameters as shown in Table 1), but we remove particular physics that have been hypothesized to be part of the mechanism of the MJO in previous studies.

3.3.1. Wind induced surface heat exchange

Emanuel (1987) suggested that enhanced evaporation to the east of the MJO convective center destabilizes the disturbance owing to the existence of basic state easterly winds in the tropics, and the observed dependence of surface fluxes on wind speed. While this idea has been questioned by subsequent studies that note that MJOs often occur in regions with basic state westerlies, and that surface fluxes may actually weaken MJOs (e.g. Lin and Johnson 1996, Haertel et al. 2008), other more recent studies that characterize the MJO as a moisture mode also emphasize the importance of wind-dependent surface fluxes by enhancing evaporation in MJO *westerlies* (Sobel and Maloney 2012). Such studies motivate an experiment with the LAM in which the wind-dependent nature of surface fluxes is turned off. For the purpose of calculating surface fluxes, a constant wind speed is assumed, equal to the average wind speed for the COARE IFA. Fig 7a shows the resulting time longitude series of rainfall. A slow moving MJO like disturbance remains, with a similar vertical structure to that for the control case (not shown). However, in this case it has a zonal wave number 2 pattern, it is weaker, and it propagates more slowly. This result suggests that wind-dependent surface fluxes are not necessary for the LAM MJOs, but they do affect MJO structure, speed, and amplitude.

3.3.2. Surface friction

It has been suggested that the MJO's mechanism of eastward propagation involves surface-friction induced low-level convergence to the east the convective center (e.g., Wang and Rui

1990). In order to find out if this is the mechanism of eastward propagation for the LAM MJO, a run is conducted in which surface friction is set to zero, but a Newtownian damping of winds *at all levels* is included. The damping time scale is roughly 5 days, consistent with the observed equivalent linear damping time of zonal winds in the MJO (Lin et al. 2005). In this case there is little change in MJO structure and propagation speed (Fig. 7b), and if anything the MJO becomes stronger with uniform wind damping as opposed to surface friction.

3.3.3. Convective momentum transport

A number of studies have hypothesized that convective momentum transport (CMT) contributes to MJO circulations and possibly the propagation of the convective center (e.g. Houze et al. 2000, Majda and Biello 2004, Moncrieff 2004). Here the term CMT is used loosely to include momentum transport by convective updrafts and downdrafts, mesoscale convective systems, and synoptic scale waves, and to include both vertical and horizontal transports. While clearly the low-resolution version of the LAM used here cannot resolve such transports, the LO convective parameterization does transport momentum vertically, which could represent vertical CMT in a crude way. To remove this parameterized CMT, a run is conducted in which parcels transported vertically by the LO scheme leave their momentum behind (i.e. in addition to swapping vertical positions, parcels swap zonal and meridional velocities). The resulting MJOs are slower and more spread out (Fig. 7c), but have similar structure, and it is not clear if the changes to the MJOs are a direct result of the lack of CMT or stem from changes to basic state winds, which include an amplification of low-level easterlies (not shown). In any event this result suggests that the CMT associated with the LO scheme is not necessary for simulating MJOs.

3.3.4 Coriolis force

One of the more interesting physics reduction experiments we conducted with the LAM involved removing the Coriolis force entirely. Owing to the relatively narrow band of high SSTs

near the Equator (Fig. 4), an equatorial intertropical convergence zone is maintained, with off-equatorial subsidence. However, in this case there is almost no basic state flow. Large-scale waves spontaneously form, propagating both eastward and westward with phase speeds greater than that of MJOs (Fig. 7d). Their vertical structures are mirror images of each other, and the structure of the eastward moving wave (Fig. 8) is very similar to that of the convectively coupled Kelvin wave (Straub and Kiladis 2003). Similarly, the structure of the westward moving wave is quite similar to that of a 2-day wave (Haertel and Kiladis 2004; not shown). This second-baroclinic, tilted wind structure (Fig. 8) is quite different from the first-baroclinic structure of MJOs simulated with the LAM (Fig. 6), and also MJOs observed in nature (e.g. Kiladis et al. 2005). This result suggests that the dominant convective organization in the absence of the Coriolis force is eastward and westward convectively coupled gravity waves, and also supports the idea that convectively coupled Rossby waves are an essential part of MJO structure (e.g., Majda and Stechman 2009).

4. Simulating the MJO with Realistic SST Patterns

In the previous section, it was shown that certain model parameters in the LO convective scheme determine the organization of tropical convection within the LAM, and in particular, whether MJOs or some sort of convectively coupled gravity wave (e.g., Kevin waves) are preferred. The MJOs discussed in that section were simulated using an idealized zonally symmetric sea surface temperature (Fig. 4) in a model with a limited meridional extent (30 S to 30 N). Moreover, unlike MJOs observed in nature, they circled the entire globe with active convection (Figs. 5,7). In this section we explore the effects of using a more realistic SST pattern and a broader domain (60 S to 60 N) on MJO genesis, structure, and evolution. While an aquaplanet configuration is still employed, realistic (Levitus annual) SSTs over oceanic locations are prescribed, with zonal interpolation of observed SSTs over continental locations. Model parameters are set the same as they are for the simulation shown in Fig. 5d, which is the control simulation with an MJO favorable swap frequency of 12.

The simulation with realistic SST patterns generates a persistant, cyclic MJO (Fig. 9a). As in nature, convection intensifies over the Indian Ocean, propagates eastward at about 5 $m\ s^{-1}$, and dissipates just east of the International Date Line. The period of the disturbance is roughly 50 days (Fig. 9a), which is also consistent with observations. The simulated MJO (Fig. 9a) is actually more regular and intense then that observed in nature (e.g., Fig. 9b). There are several possible reasons for this difference. First, the swap frequency parameter was tuned to generate a strong MJO (Section 3.2), and may actually parameterize updrafts and downdrafts to be more penetretative then they are in nature. Second, the model uses a constant radiative cooling, which does not damp local temperature perturbations as much as a more realistic cooling. Third, it is possible that the aquaplanet configuration, along with the spatially limited domain, might be conducive to stronger MJOs.

Figure 10 presents a composite vertical structure of the 6 MJOs shown in Fig. 9a, which was constructed by computing time averages in a cooridinate system moving with the MJO precipitation center. Ahead of the most intense convection there is a broad region of lower tropospheric easterlies, and trailing the precipitation a more narrow area of lower tropopheric westerlies that tilts westward with height (Fig. 10a). Upper tropospheric flow is out of phase with lower tropospheric flow, and the lower tropospheric easterlies are connected with the upper tropospheric easterlies in a narrow region near the precipitation center. The most prominant temperature feature is an upper-level warm anomaly peaking between 300 and 400 hPa near the precipitation center that tilts downward toward the east (Fig. 10b), with cooler air to the west and beneath it. The atmosphere moistens ahead of the deep convection at low-levels first, transitioning to a deep and intense moisture anomaly that accompanies the convective center, and followed by deep tropospheric dryness (Fig 10c). Convective heating also begins in the lower troposphere ahead of the precipitation center, with deeper heating to the west, producing a tilted heating anomaly (Fig. 10d). Overall, the gross vertical structures of wind, temperature, moisture and heating are consistent with those observed by Kiladis et al. (2005), with a few minor differences attributable to the idealized nature of the simulations.

The horizontal flow features include a pair of cyclonic gyres that straddle the equator to the west of the precipitation center, and which are associated with westerlies that flow into the most intense convection (Fig 11a). At upper levels there is a classic quadrapole gyre, with a pair of anticyclone gyres just to the west and poleward of the precipitation center, and a pair of cyclonic gyres on either side of the equator much further to the east. The numerous realistic aspects of the simulated convective disturbances including their period, location of origin and dissipation, rate of propagation, vertical structures of zonal wind, temperature, moisture and heating, as well as hoizontal flow structures at low and upper levels, all provide evidence that the LAM is indeed simulating the MJO. Moreover the fact that the MJO is spontaneously generated in a very low resolution and idealized model has a number of implications for its dynamics, which are discussed in Section 7.

5. Sensitivity to Radiation

One idealized aspect of the simulations presented above is that they include a very simple treatment of atmospheric radiation--a prescribed constant cooling in the troposphere with a relaxation to observed stratospheric temperatures. This section explores how simulations change when a more realistic radiation scheme is used based on that proposed for testing general circulation models by Frierson et al. (2006). While the new scheme is still idealized, it is useful for testing sensitivities to three potentially important aspects of atmospheric radiation for the MJO: 1) vertical structure of radiative cooling; 2) radiative damping of tropospheric temperature perturbations; and 3) moisture dependent radiative destabilization of the MJO.

5.1 New radiation scheme and other model improvements

Our radiation scheme is a modified version of that described by Frierson et al. (2006), and the reader is referred to that study for details on the radiative transfer equations and the overall framework of the scheme. Three modifications to the Frierson et al. scheme are used for this study: 1) a moisture dependent equation for total optical depth, 2) a modified vertical structure

function for optical depth, and 3) and a reduction in the total radiative flux. Below we provide details on these modifications and also describe other changes made to the LAM for the radiation sensitivity tests.

Our new equation for total optical depth is as follows:

$$\tau_0 = \tau_{0_b} + \tau_{0_w}\left(\frac{W}{40mm}\right) \tag{3}$$

where τ_0 is the total optical depth, τ_{0_b} is the baseline optical depth, τ_{0_w} represents the sensitivity of optical depth to atmospheric moisture, and W is the precipitable water in *mm*. The new vertical structure function has the form

$$\tau = \tau_0\left(\frac{p}{p_0}\right)^n \tag{4}$$

where p is pressure, p_0 is the surface pressure, and n is an integer. For the purposes of calculating radiative fluxes we use:

$$B = \mu\sigma T^4 \tag{5}$$

where B is the radiative flux, σ is the Stefan-Boltzman constant, and μ is used to reduce the intensity of the radiative cooling to account for the lack of short wave forcing in the model and for regions of the infrared spectra in which there is little absorption or emission (i.e. atmospheric windows).

All parameters are tuned simultaneously to generate as realistic vertical structure and amplitude for radiative cooling as possible in this simple framework. The values used for the simulations presented below are $\tau_{0_b} = 3$, $\tau_{0_w} = 7$, $n = 2$, and $\mu = 0.5$. Figure 12 compares the net radiative forcing in the model over the western Pacific warm pool to that estimated by L'Ecuyer et al. (2010). Note that the model produces a peak cooling at the same height as the observationally based estimate, and that the overall amplitude of the radiative cooling is also

similar. We use a more gradual taper of optical depth with height ($n = 2$) than that used by Frierson et al. (2006) to achieve this realistic vertical structure, which is consistent with the idea that not only water vapor, but also cloud particles and other greenhouse gases make important contributions to longwave optical depth.

In addition to including the new radiation scheme, more narrow columns for the LO scheme are used for the simulations presented below, which yields more realistic zonal wind structure at lower resolution. These changes to the model require retuning a number of other model parameters, which are listed in Table 2. All of our modifications represent a gradual shift towards realism, while still maintaining the simplicity of the LAM, which aids in dynamical interpretation of simulations.

5.2 Simulation of MJOs

With the new radiation scheme, the LAM continues to produce robust MJOs. For example, Fig. 13 shows a simulation in which a series of MJOs form, with vertical and horizontal structures compared with observations in Figs. 14-17. As before, locations of genesis and dissipation of the active convection are similar to those in observations (Figs. 13, 9b). One aspect of the composite MJO zonal wind structure (Fig. 14) that is more realistic than before is that low-level easterlies extending eastward from the convective center are more localized to the region of convection. This might be caused by temperature damping associated with the radiation scheme, which damps the first baroclinic Kelvin wave extending eastward from the convective center. The same general temperature pattern is seen in the runs with constant cooling (Fig. 10b) and with the new radiation scheme (Fig. 15a), which is consistent with observations (Fig. 15b). The new radiation scheme increases the moistening ahead of the convective center at low levels (compare Fig. 16a to Fig. 10c), but it is still not as deep as in observations (Fig. 16b). As is discussed in the appendix, using a higher model resolution yields deeper and more realistic moistening ahead of the MJO. The new radiation scheme produces quadrapole gyres (Fig. 17) that have a more realistic structure, with the eastern gyres more

localized to the region of intense convection. We conclude that while the new radiation scheme is not necessary for simulating the most fundamental dynamics of the MJO, it does improve several details of MJO structure.

5.3 Radiative Destabilition of the MJO

One theory of the MJO is that a reduced longwave cooling in the convectively active region contributes to its instability (Raymond 2001). In order to test this concept for the LAM MJO, we modify our radiation scheme to be moisture insensitive by using the following equation for optical depth:

$$\tau_0 = \tau_{0_b} + \tau_{0_l}(90^o - \phi)/90^o \tag{6}$$

where τ_{0_l} is set equal to τ_{0_w} (defined above) and ϕ is latitude. This yields a similar overall pattern to optical depth with high values near the equator and low values near the poles, but which is insensitive to local atmospheric water vapor variations (and more like the Frierson et al. 2006 scheme). It turns out that making this change has very little impact on the MJO. Figure 18 shows that MJOs with similar amplitudes, regions of formation and dissipation, and horizontal and vertical structures develop with the "gray" version of the radiation scheme. This result, along with the simulations presented in Sections 3-4, make it clear that radiation instability is neither necessary for the LAM MJO nor part of its most fundamental dynamics.

6. Relationship between MJO Activity and Basic State

In this section we examine the relationship between MJO activity and time average precipitation patterns and zonal wind structure within the LAM. These runs employ the version of the model described in the previous section (i.e. with the new radiation scheme). Strong MJO activity is accompanied by heavy precipitation over the Indian Ocean and west Pacific, a relatively weak eastern Pacific/Atlantic Intertropical Convergence Zone (ITCZ), and westerly winds aloft over the equator.

6.1 Time Average Precipitation

Figure 19a shows the average rainfall for the simulation with a series of MJOs depicted in Figs. 13-17. As in the Global Precipitation Climatology Project (GPCP; Huffman et al. 2001) observed annual rainfall map (Fig. 19b), there is a region of heavy rainfall straddling the equator from the eastern Indian Ocean to just east of the Dateline with local maxima in both the eastern and western portions. There is also an ITCZ extending eastward over the eastern Pacific, across what would be South America (if the model had continents), and into the Atlantic. In the run with strong MJOs (Fig. 19a) the rainfall to the east of the Dateline is weaker than observed (Fig. 19b). However, when the model's evaporation parameter is reduced, which slightly weakens the MJO, the eastern Pacific/Atlantic ITCZ is enhanced (Fig. 19c) becoming more like the observed ITCZ (Fig. 19b). In the run with MJO-favorable parameters (Figs. 13-17,19a), the MJO is actually slightly more regular and intense than typically observed in nature, and the subsidence associated with the first-baroclinic forced Kelvin wave to its east might be suppressing convection within the eastern Pacific/Atlantic ITCZ (Fig. 19a). Overall, the simulated tropical rainfall patterns (Figs. 19a,c) are more realistic then expected for such an idealized low-resolution model with no continents or orography, which could mean that the LO parameterization also has advantages for producing realistic precipitation patterns. In particular, these simulations exhibit no sign of the double ITCZ problem commonly observed in climate models, and there is also no evidence of an unrealistic heavy rain band from 10^o to 20^o N between 60^o and 160^o E, which has been found in conventional climate models tuned to have strong MJOs (Kim et al. 2011).

6.2 Zonal wind structure

Figure 20a shows zonal average zonal winds for the LAM run with MJO-favorable parameters (Figs. 13-17). At low levels winds are similar to those observed in nature: there are weak easterlies from $30^o S$ to $30^o N$ that peak slightly above 5 $m\ s^{-1}$ near the surface around $15^o N/S$, and westerlies that increase in amplitude with height at midlatitudes (Figs. 20a-b).

Simulated upper-level mid-latitude zonal jets are also similar to observed jets, with maximum amplitudes between 25 and 35 $m\ s^{-1}$ located near 200 hPa (Figs. 20a-b). However, one feature of the LAM simulation that is noticeably different from observations is the presence of westerlies or superrotation in the upper troposphere over the equator. Numerous LAM simulations we have conducted suggest that there is a correlation between these westerlies and MJO activity. For example, when the entrainment/detrainment parameter is reduced, causing weaker MJOs, the upper-level westerlies weaken (Fig. 20c). While it seems likely that momentum transport from the MJO contributes to this superrotation (e.g., Caballero and Huber 2010), it is unclear if the superrotation also helps to destabalize the MJO. Another factor that contributes to the upper level westerlies over the equator is the low resolution of the LAM; as is discussed in the appendix upper-level westerlies weaken and simulated zonal winds become more like observed winds in general when the model resolution is increased.

6.3 Temperature and moisture profiles

Some of the parameter changes that make relatively large changes to MJO activity, precipitation patterns, and zonal wind structure, make comparatively small changes to profiles of moisture and temperature in the tropics. For example, Figures 21a-b show profiles of temperature and humidity respectively over the western Pacific warm pool (solid lines) compared to observed profiles (dashed lines) for a run with reduced mixing and a realitively weak MJO. These profiles are quite close to those for the run with an active MJO (Fig. 3).

7. Summary and Discussion

In this study we show that a novel Lagrangian atmospheric model can generate surprisingly realistic MJOs, even at very low resolution. The model employs a unique convective parameterization (LO), in which overlapping air parcels exchange vertical positions in convectively unstable regions. With careful tuning, the LO scheme generates robust MJOs in a variety of aquaplanet settings: a tropical channel model with zonally symmetric SST forcing, a

tropical/midlatitude model with realistic SST patterns, and a near global model with realistic SSTs and a more realistic radiation scheme.

A key model parameter for simulating MJOs is the vertical position swap frequency, with the most frequent and strongest MJOs occuring when LO is applied many times per model time step. This result suggests that including effects of pennetrative updrafts and downdrafts might be an important part of simulating the MJO. Idealized experiments aimed at identifying the most fundamental dynamics of the MJO show that convective entrainment/detrainment and the Coriolis force are necessary for simulating MJOs using the LAM, and that surface friction, wind-dependent surface fluxes, convective momentum transport, and interactive radiation are not necessary, but can affect MJO structure, intensity, and propagation speed. While the LAM can simulate MJOs with a constant radiative cooling, MJO intensity and structure are more realistic when radiative cooling depends on longwave optical depth and temperature.

While these results are certainly encouraging in terms of illustrating several potental advantages of the LO convective scheme for simulating tropical convection, their greater importance might lie in what they say about the dynamics of the MJO. The simulations presented here show that robust MJOs with realistic vertical and horizontal structures can be simulated with a model that is only capable of resolving planetary scale circulations, with very simple moisture-independent radiation, and which parameterizes only the bulk effects of convective entrainment/detrainment and microphysics in a simple way. This suggests that the most fundamental dynamics of the MJO are a coupling between moist convection and planetary-scale Rossby and/or Kelvin waves, in which entrainment into penetrative convective plumes is a key physical process. They also establish that the physics of the convection/wave coupling in the MJO are relatively easy to parameterize in a Lagrangian framework, and provide motitivation for further development of climate models using this framework.

Acknowledgements. We thank Dargen Frierson for suggesting the use of the new radiation scheme. We thank Raymond Shaw for advice on implementing cloud water into the microphysics. This research was supported by NSF Grant AGS-1116885.

Appendix: Sensitivity of MJO Simulations to Model Resolution

For the bulk of the simulations presented in this paper we use a very low model resolution (i.e. an equivalent Eulerian resolution on the order of 1000 *km*), which is sufficient for resolving planetary scale circulations, but not synoptic scale circulations. As is mentioned above, the fact that the MJO can be simulated with such a low resolution is an important result in terms of what it implies about the dynamics of the MJO. Moreover, using this low resolution reduces the computational requirements of the numerous simulations needed to tune model parameters. However, it is also important to establish that the disturbances we identify as MJOs are not some sort of grid-scale numerical artifact. This section explores the effects of doubling model resolution in latitude and longitude, so that individual parcels become 4 times less massive. We present results from a higher resolution LAM run, which has similar model parameters (Table 3), to those for the control MJO simulation shown in Figs. 13-17 (Table 2).

At the higher resolution in the MJO-favorable parameter regime, persistent and cyclic MJOs develop (Fig. A1a). With the higher resolution individual MJO envelopes can contain multiple Kelvin waves as well as high frequency westward propagating disturbances reminiscent of 2-day waves (Takayabu et al. 1996; Haertel and Kiladis 2004). However, the overall MJO structure (Fig. A1b-e,g), including regions of formation and dissipation, propagation speed, and horiozontal and vertical structure, is similar to that generated with the low resolution version of the LAM (Figs. 13-17). The most significant change to the MJO vertical structure at the higher resolution is a deeper and more realistic moistening ahead of the MJO (Fig. A1e), which might be a consequence of the embedded smaller scale disturbances.

The other important change, which might be dependent on a more realistic representation of baroclinic waves, is a more realistic zonal wind pattern with weaker westerlies at upper levels in equatorial regions (Fig. A1f). This result suggests that the stronger equatorial superrotation seen in the lower resolution simulation (Fig. 20a) is partly a consequence of the low resolution. In fact, in some higher resolution runs with weaker MJOs the superrotation mostly disappears (not shown).

References

Barrett, B. S. and L. M. Leslie, 2009: Links between tropical cyclone activity and Madden Julian Oscillation phase in the North Atlantic and northeast Pacific basins. *Mon. Wea. Rev.*, **137**, 727-744.

Blade, Dennis L. Hartmann, 1993: Tropical intraseasonal oscillations in a simple nonlinear model. *J. Atmos. Sci.*, **50**, 2922-2939.

Caballero R. and M. Huber, 2010: Spontaneous transition to superrotation in warm climates simulated by CAM3. *Geophys. Res. Let.*, **37**, L11701, doi:10.1029/2010GL043468, 2010.

Cassou C., 2008: Intraseasonal interaction between the Madden-Julian Oscillation and the North Atlantic Oscillation. *Nature*, **455**, 523-527. DOI:10.1038/nature07286.

Ciesielski, P. E., R. H. Johnson, P. T. Haertel, J. Wang, 2003: Corrected TOGA COARE sounding humidity data: Impact on Convection and Climate, *J. Climate*, **16**, 2370-2384.

Emanuel, Kerry A., 1987 An air-sea interaction model of intraseasonal oscillations in the tropics. *J. Atmos. Sci.*, **44**, 2324-2340.

Emanuel, K. A., J. D. Neelin, and C. S. Bretherton, 1994: On large-scale circulations in convecting atmospheres. *Q. J. R. Meteorol. Soc.*, **120**, 1111-1143.

Fedorov, A.V., 2002: The response of the coupled tropical ocean-atmosphere to westerly wind bursts. *Q. J. Roy. Meteorol. Soc.*, **128**, 1-23.

Fedorov, A.V., Harper, S.L., Winter, B. and Wittenberg, A., 2003: How predictable is El Nino? *Bull. Amer. Meteorol. Soc.*, **84**, 911-919.

Frierson, D. M. W, I. M. Held, and P. Zuria-Gotor, 2006: A gray radiation aquaplanet moist GCM. Part I: Static stability and eddy scale. *J. Atmos. Sci.*, **63**, 2548-2566.

Grabowski, W. W., 2001: Coupling cloud processes with the large-scale dynamics using the cloud-resolving convection parameterization (CRCP). *J. Atmos. Sci.*, **58**, 978-997.

Haertel, P. T., 2012: A Lagrangian method for simulating geophysical fluids. AGU Book Series *Lagrangian Modeling of the Atmosphere* (in press).

Haertel, P. T. and D. A. Randall, 2002: Could a pile of slippery sacks behave like an ocean? *Mon. Wea. Rev.,* **130,** 2975-2988.

Haertel, P. and K. H. Straub, 2010: Simulating convectively coupled Kelvin waves using Lagrangian overturning for a convective parameterization. *Q. J. Royal Met. Soc.*, **136**, 1598-1613.

Haertel, P. T. and G. N. Kiladis, 2004: Dynamics of two day equatorial waves, *J. Atmos. Sci.*, **61**, 2707-2721.

Haertel, P. and A. Fedorov, 2012: The Ventilated Ocean. *J. Phys. Oceanogr.* **42**, 141-164. parameterization. *Q. J. Royal Met. Soc.*, **136**, 1598-1613.

Haertel, P. T., L. Van Roekel, T. Jensen, 2009: Constructing an idealized model of the north Atlantic Ocean using slippery sacks, *Ocean Modeling*, **27**, 143-159.

Haertel, P. T., D. A. Randall and T. G. Jensen, 2004: Simulating upwelling in a large lake using slippery sacks, *Mon. Wea. Rev.*, **132**, 66-77.

Haertel, P. T., G. N. Kiladis, T. Rickenbach, and A. Denno., 2008: Vertical mode decompositions of 2-day waves and the Madden-Julian oscillation, *J. Atmos. Sci.,* **65**, 813-833.

Kessler, W. S., 2001: EOF representations of the Madden Julian Oscillation and its connection with ENSO. *J. Climate*, **14**, 3055-3061.

Kessler, W. S., R. K., 2000: Rectification of the Madden Julian Oscillation into the ENSO Cycle. *J. Climate*, **13**, 3560-3575.

Khairoutdinov, M. F., and D. A. Randall, 2001: A cloud-resolving model as a cloud parameterization in the NCAR Community Climate System Model: Preliminary results. *Geophys. Res. Lett.*, **28**, 3617-3620.

Kiladis, G. N., K. H. Straub, and P. T. Haertel, 2005: Zonal and vertical structure of the Madden-Julian oscillation, *J. Atmos. Sci.*, **62**, 2790-2809.

Hendon and Liebmann, 1994: Organization of convection within the Madden-Julian oscillation. *J. Geophys. Res.*, **99**, 8073-8083.

Houze, R. A., Jr., S. S. Chen, D. E. Kinsmill, Y. Serra, and S. E. Yuter, 2000: Convection over the Pacific warm pool in relation to the atmospheric Kelvin-Rossby wave. *J. Atmos. Sci.*, **57**, 3058-3089.

Huffman, G. J., R. F. Adler, M. M. Morrissey, D. T. Bolvin, S. Curtis, R. Joyce, B. McGavock, and J. Susskind, 2001: Global precipitation at one-degree daily resolution from multisatellite observations. *J. Hydrometeor.*, **2**, 36-50.

Kim, D., A. H. Sobel, E. D. Maloney, D. M. W. Frierson, I.-S. Kang, 2011: A Systematic Relationship between Intraseasonal Variability and Mean State Bias in AGCM Simulations. J. Climate, 24, 5506-5520.

Kim, D., A. H. Sobel, E. D. Maloney, D. M. W. Frierson, I.-S. Kang, 2011: A Systematic Relationship between Intraseasonal Variability and Mean State Bias in AGCM Simulations. *J. Climate*, **24**, 5506-5520.

Lau, K. M., L. Peng, 1987: Origin of low-frequency (intraseasonal) oscillations in the tropical atmosphere. Part I: basic theory. *J. Atmos. Sci.*, **44**, 950-972.

L'Ecuyer T. S. and G. McGarragh, 2010: A 10-year climatology of tropical radiative heating and its vertical structure from TRMM observations. *J. Climate*, **23**, 519-541.

Lin, X. and R. H. Johnson, 1996: Kinematic and thermodynamic characteristics of the flow over the western Pacific warm pool during TOGA COARE. *J. Atmos. Sci.*, **53**, 695-715.

Lin, J.-L., M. Zhang, B. Mapes, 2005: Zonal momentum budget of the Madden Julian Oscillation: The source and strength of equivalent linear damping. *J. Atmos. Sci.*, **62**, 2172-2188.

Lin, J.-L., G. N. Kiladis, B.E. Mapes, and 13 others, 2006: Tropical intraseasonal variability in 14 IPCC AR4 climate models. Part I: Convective signals. *J. Climate*, **19**, 2665-2690.

Lorenz, D. J., D. L. Hartmann, 2006: The effect of the MJO on the North American Monsoon. *J. Climate*, **19**, 333-343.

Maloney, E. D. and D. L. Hartmann 2000: Modulation of hurricane activity in the Gulf of Mexico by the Madden-Julian Oscillation. *Science*, **287**, 2002-2004.

Madden, R. and P. Julian, 1971: Detection of a 40-50 day oscillation in the zonal wind in the tropical pacific. *J. Atmos. Sci.*, **702**, 702-708.

Madden, R. and P. Julian, 1972: Description of global-scale circulation cells in the tropics with a 40-50 day period, *J. Atmos. Sci.*, **29**, 1109-1123.

Madden, R. A. and P. R. Julian, 1994: Observations of the 40-50 day tropical oscillation--A review. *Mon. Wea. Rev.*, **122**, 814-837.

Majda, A. J. and J. A. Biello, 2004: A multiscale model for tropical intraseasonal oscillations. *Proc. Nat. Acad. Sciences*, **101**, 4736-4741.

Majda, A. J. and S. N. Stechmann, 2009: The skeleton of tropical intraseasonal oscillations. *Proc. Nat. Acad. Sciences*, **106**, 8417-8422.

Moncrieff, M. W., 2004: Analytic representation of the large-scale organization of tropical convection. *J. Atmos. Sci.*, **61**, 1521-1538.

Nakazawa, T., 1988: Tropical super clusters within intraseasonal variations over the western Pacific. *J. Meteor. Soc. Japan*, **66**, 823-839.

Neale, R. B. and B. J. Hoskins, 2000: A standard test for AGCMs including their physical parameterizations: I: the proposal, *?Atmos. Sci. Let.*, **1**, 101-107.

Raymond, David J., 2001: A new model of the Madden-Julian Oscillation. *J. Atmos. Sci.*, **58**, 2807-2819.

Sobel, A. and E. Maloney, 2012: An idealized semi-empirical framework for modeling the Madden Julian Oscillation. *J. Atmos. Sci.*, **69**, 1691-1705.

Straub, K. H. and G. N. Kiladis, 2003c: The observed structure of convectively coupled Kelvin waves: comparison with simple models of coupled wave instability. *J. Atmos. Sci.*, **60**, 1655-1668.

Takayabu, Y. N., K. M. Lau, and C. H. Sui, 1996: Observation of a quasi-2-day wave during TOGA COARE. *Mon. Wea. Rev.*, **124**, 1892-1913.

Thayer-Calder, Katherine and David A. Randall, 2009: The Role of Convective Moistening in the Madden-Julian Oscillation. *J. Atmos. Sci.*, **66**, 3297-3312.

Van Roekel, L., T. Ito, P. Haertel, and D. Randall, 2009: Lagrangian analysis of the meridional overturning circulation in an idealized ocean basin. *J. Phys. Oceanogr.* **39**, 2175-2193.

Vecchi, G. A and N. A. Bond, 2003: The Madden-Julian Oscillation (MJO) and northern high latitude wintertime surface air temperatures. *Geophys. Res. Let.*, **31**, LO4104, doi:10.1029/2003GL018645.

Wang, B., 2005: Theory, in Intraseasonal Variability in the Atmosphere-Ocean Climate System, edited by W. K.-M. Lau and D. Waliser, chap. 10, pp. 307-351, Springer, New York.

Wang, B. and H. Rui, 1990: Dynamics of the coupled moist Kelvin-Rossby wave on an equatorial β-plane. *J. Atmos. Sci.*, **47**, 397-413.

Webster, P. J. and R. Lukas, 1992: TOGA COARE: The Coupled Ocean-Atmosphere Response Experiment. *Bull. Amer. Meteor. Soc.*, **73**, 1377-1416.

Weickmann, K. M., G. R. Lussky, and J. E. Kutzbach, 1985: Intraseasonal (30-60 day) fluctuations of outgoing longwave radiation and 250 mb streamfunction during northern winter. *Mon. Wea. Rev.*, **113**, 941-961.

Wu, M. L. C, S. Schubert, N. E. Huang, 1999: The development of the South Asian Summer Monsoon and the Intraseasonal Oscillation. *J. Climate*, **12**, 2054-2075.

Zhang, C., 2005: Madden Julian Oscillation, *Rev. Geophys.*, **43**, RG2003, DOI 10.1029/2004RG000158, 36 pages.

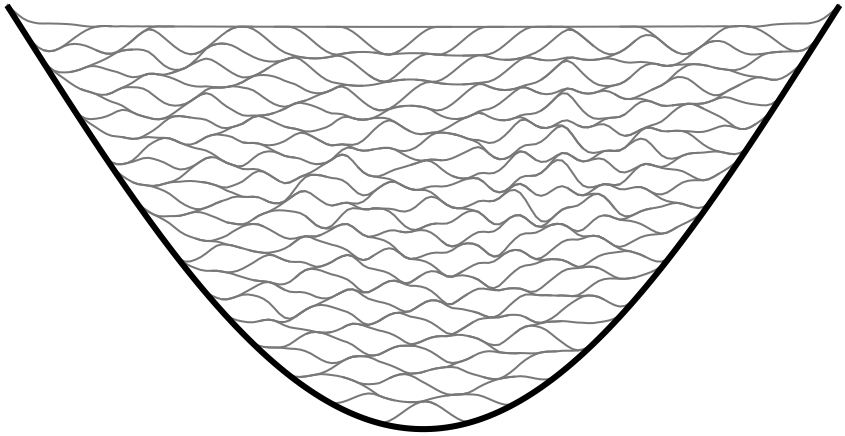

Figure 1. An illustration of the conforming parcel concept: a collection of fluid parcels in a basin (from Haertel and Fedorov 2012).

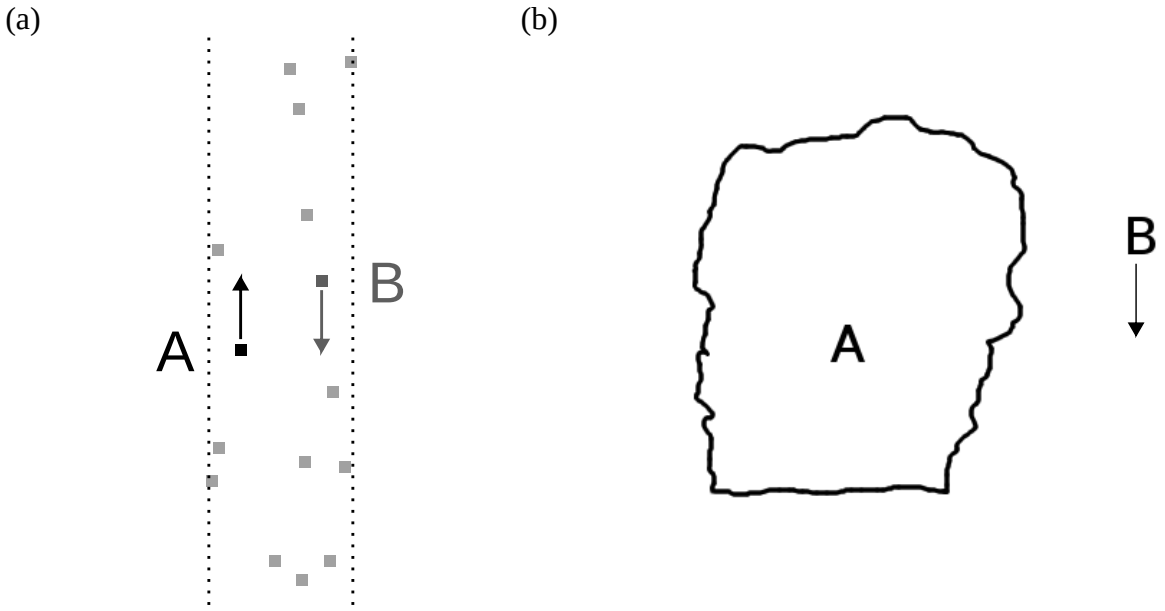

Figure 2. The LO convective parameterization (from Haertel and Straub 2010). (a) A column of parcel centers from an actual Lagrangian simulation. Points A and B satisfy the check for the convective parameterization--exchanging their vertical positions leads to a higher potential temperature for the rising parcel. (b) The physical processes the swap parameterizes: parcel A represents air rising in convective clouds and parcel B represents air sinking around the clouds.

(a)

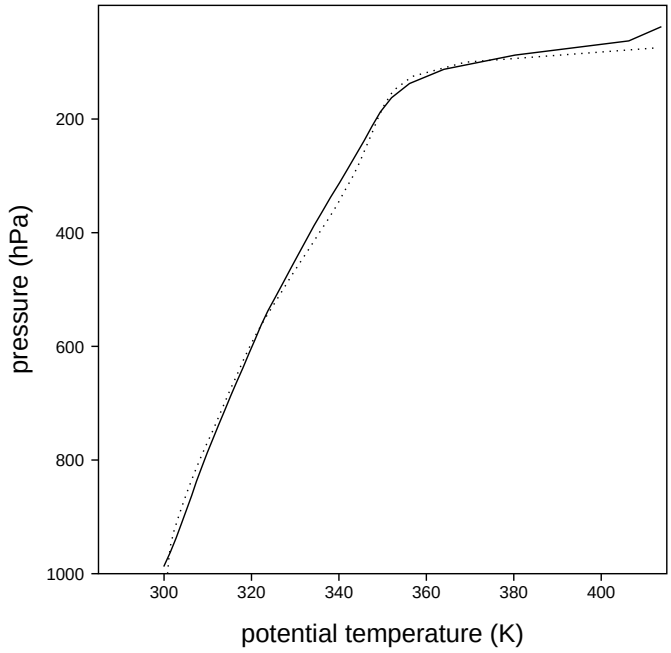

(b)

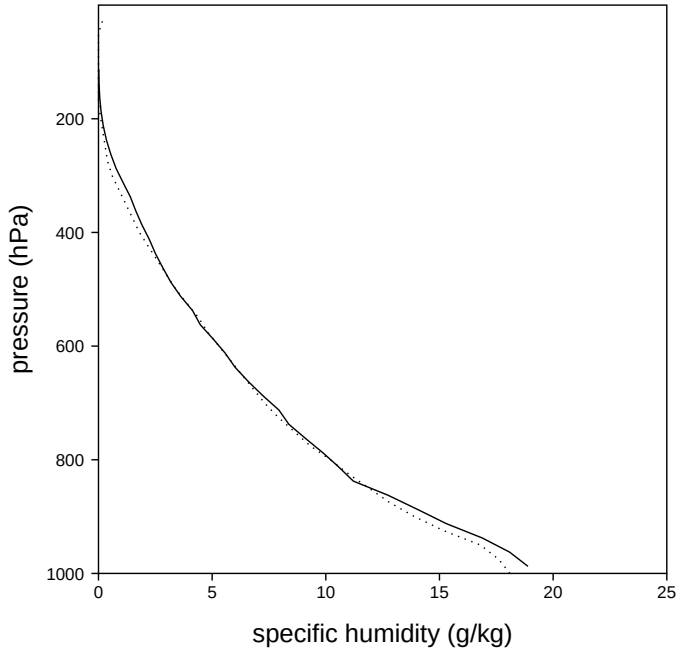

Figure 3. Simulated profiles of (a) potential temperature and (b) specific humidity for the simulation of MJOs with a modified radiation scheme (solid lines). Observed profiles for COARE IFA (Ciesielski et al. 2003) are shown as dotted lines in each panel.

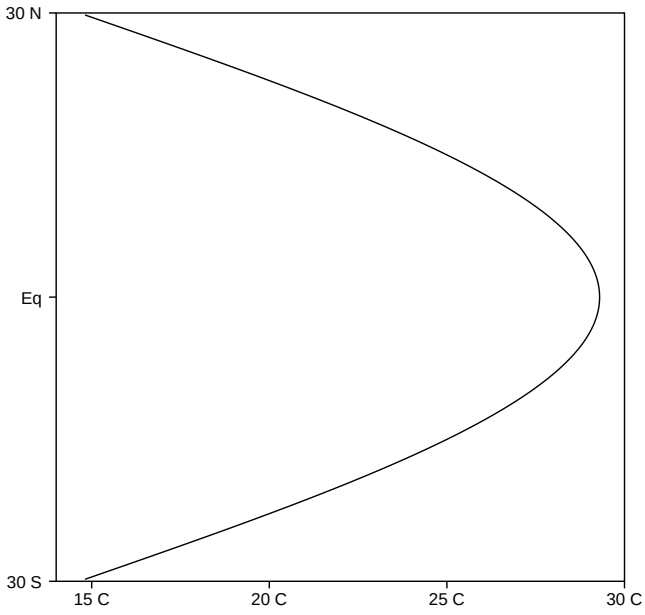

Figure 4. Prescribed sea surface temperature for the tropical channel simulations of MJOs.

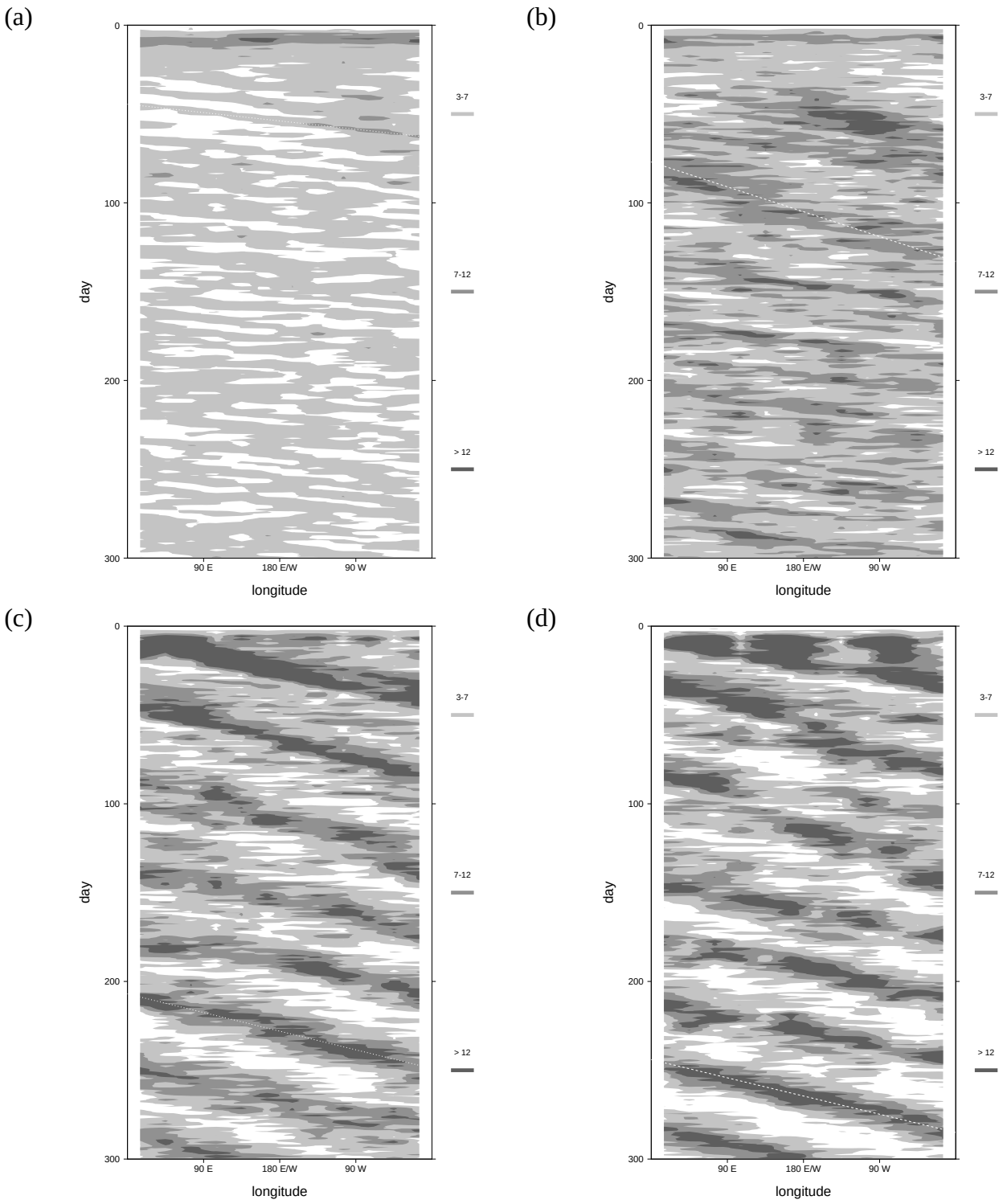

Figure 5. Time pressure series of rainfall (mm/day) for tropical channel simulations with LO swap frequencies (SFs) of (a) 1, (b) 3, (c) 7 and (d) 12. Notice the transition from a Kelvin wave regime to an MJO regime as SF is increased. The phase velocities of the dotted lines shown in panels (a-d) are 24, 8, 11, and 12 $m\ s^{-1}$ respectively.

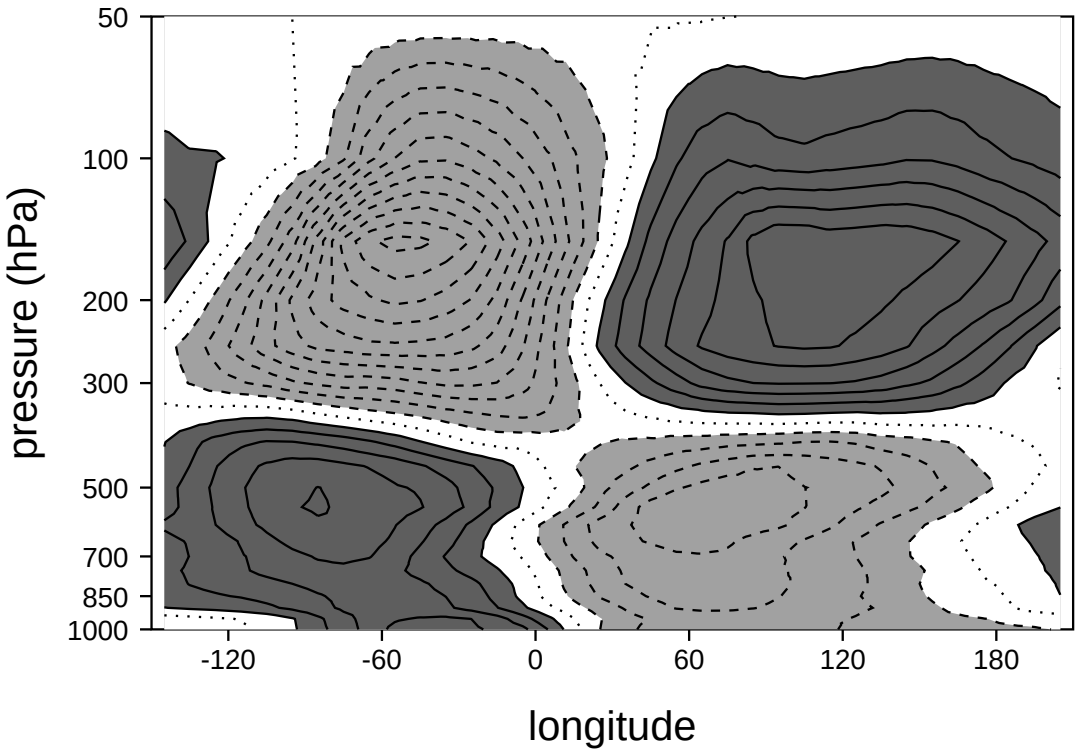

Figure 6. Composite zonal wind structure (1 $m\ s^{-1}$ contour interval) of the MJO marked with a dashed line in Fig. 5d. The coordinate system is centered on the region of precipitation. Note the first baroclinic wind structure, with lower-tropospheric easterlies and upper-tropospheric westerlies ahead (to the east) of the precipitation center, with opposite wind perturbations trailing the precipitation center.

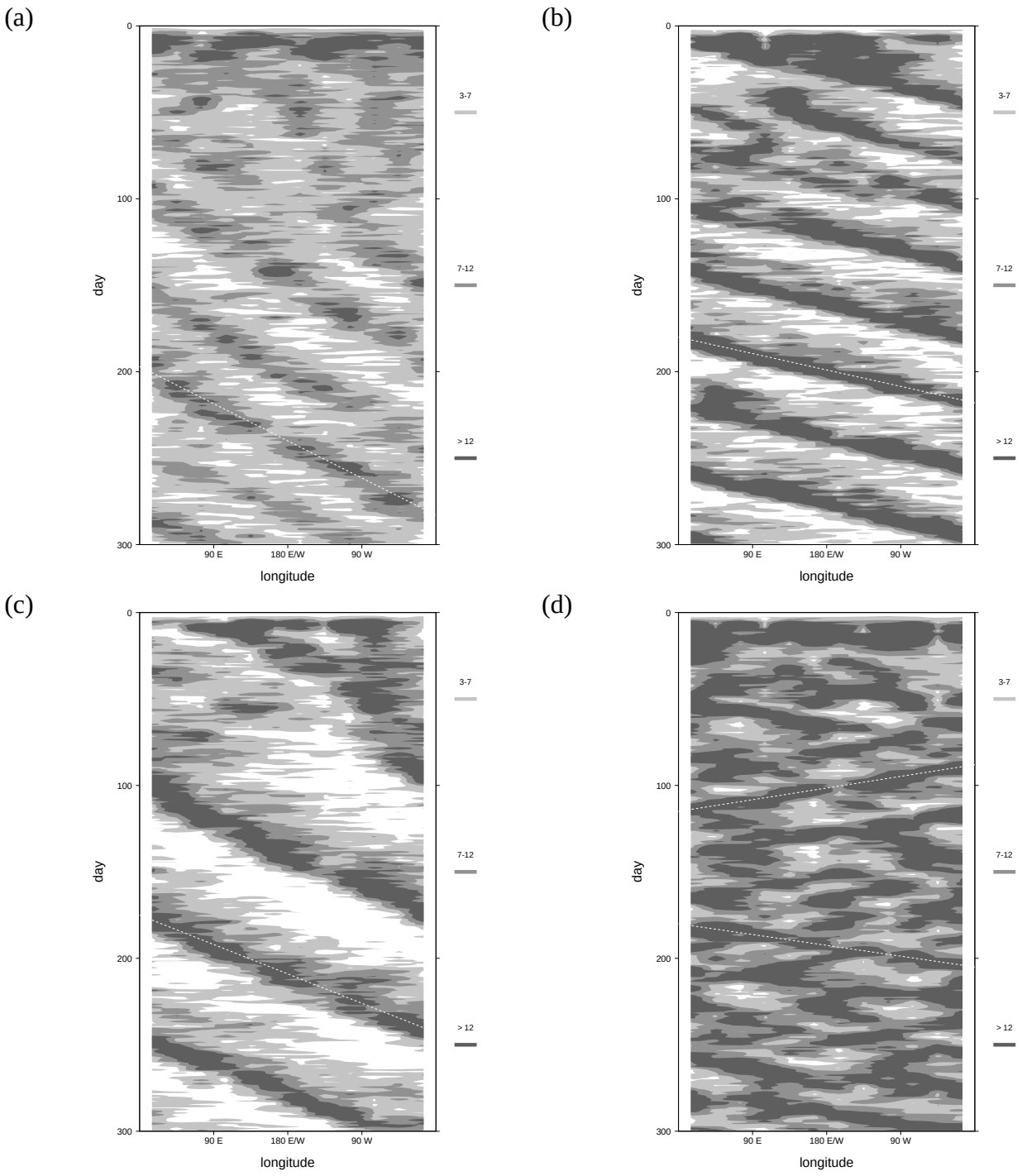

Figure 7. Time longitude series of rainfall for four physics reduction experiments: (a) wind enhanced evaporation, (b) surface friction, (c) convective momentum transport, (d) Coriolis force. The MJO continues to exist with altered structure and/or intensity for experiments (a-c), but in experiment (d) there are only convectively coupled gravity waves that propagate rapidly in eastward and westward directions, and can be distinguished from MJOs by vertical structure. The phase velocities of the dotted lines shown in panels (a-d) are 5, 12, 7, and 18 $m\ s^{-1}$ respectively.

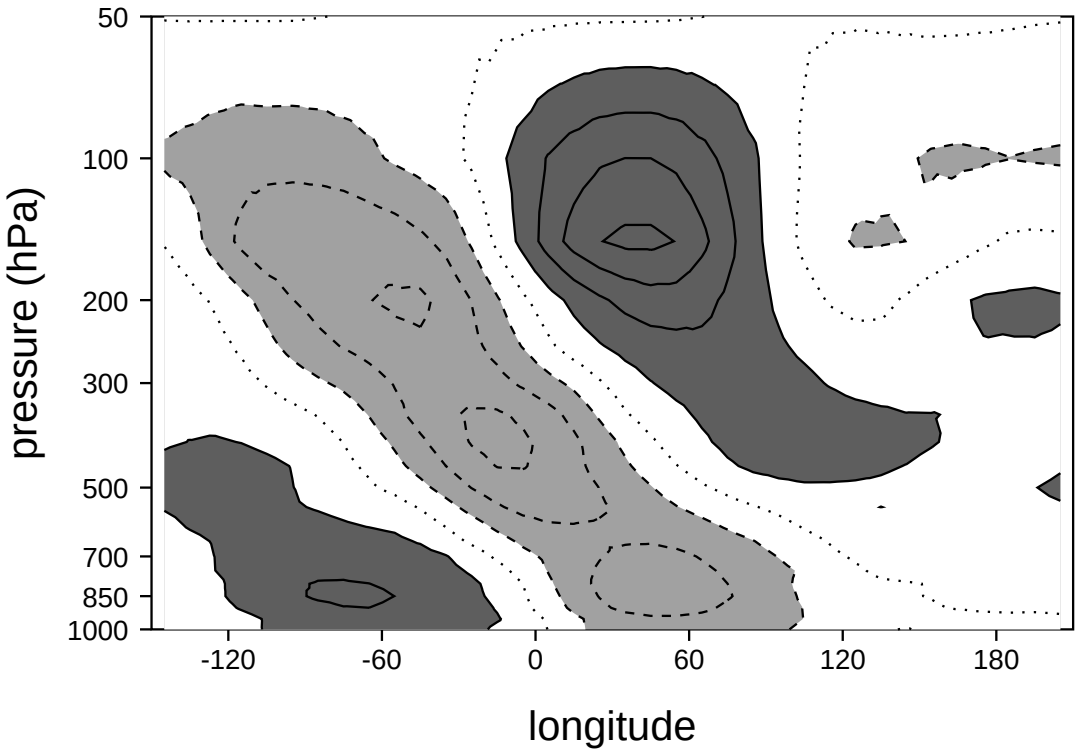

Figure 8. Composite zonal wind structure (1 $m\ s^{-1}$ contour interval) of the eastward propogating convectively coupled gravity wave marked with a dashed line in Fig. 7d. The coordinate system is centered on the region of precipitation. Note the tilted wind perturbations along with a strong signal of second baroclinic wind structure, with maxima in lower-, mid-, and upper-troposphere, which is characteristic of convectively coupled equatorial waves such as 2-day waves and Kelvin waves.

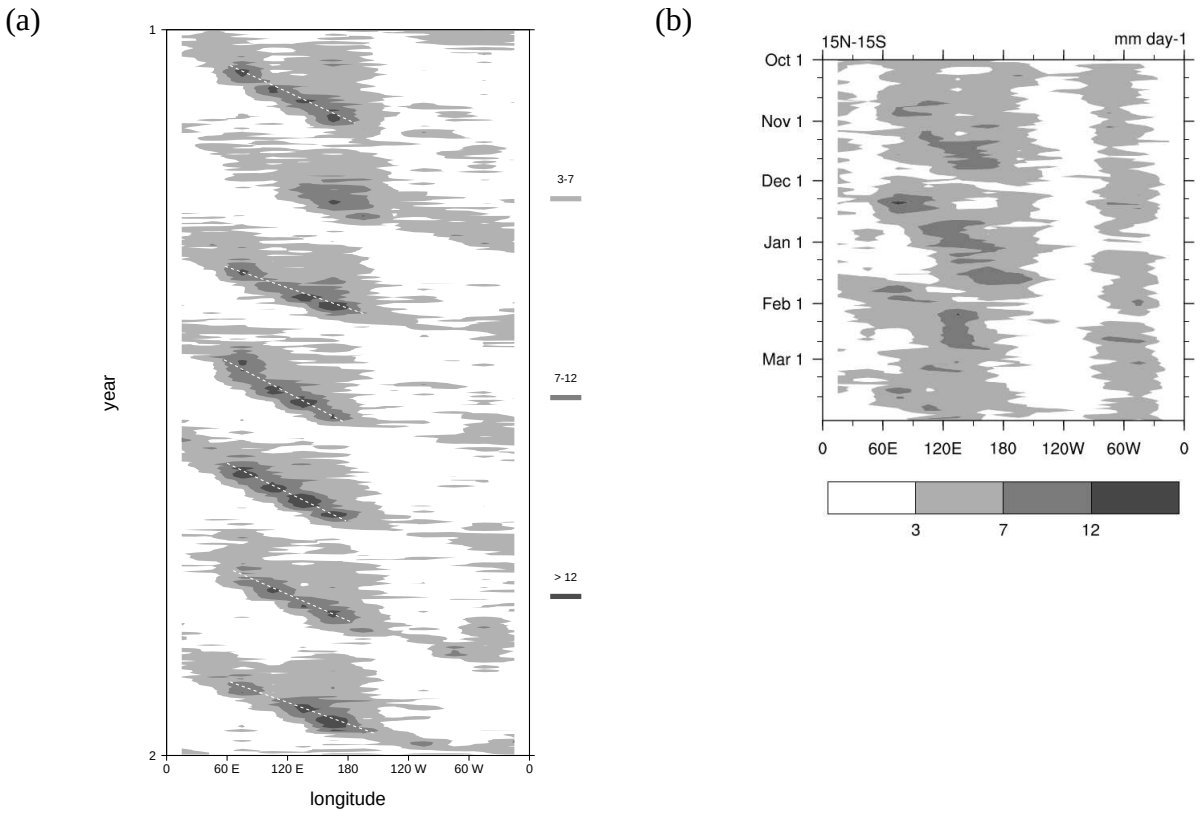

Figure 9. (a) Time longitude series of rainfall (mm/day) for a LAM simulation with realistic prescribed SSTs and constant radiative cooling. Dotted lines trace out approximate paths of MJOs, and are used to construct composite vertical and horizontal structures shown in Figures 10-11. The average phase speed is 6 $m\ s^{-1}$. (b) Observed time series of rainfall (GPCP) for a series of MJOs that occurred between October 2007 and March 2008 with a resolution reduced to that of the LAM simulation.

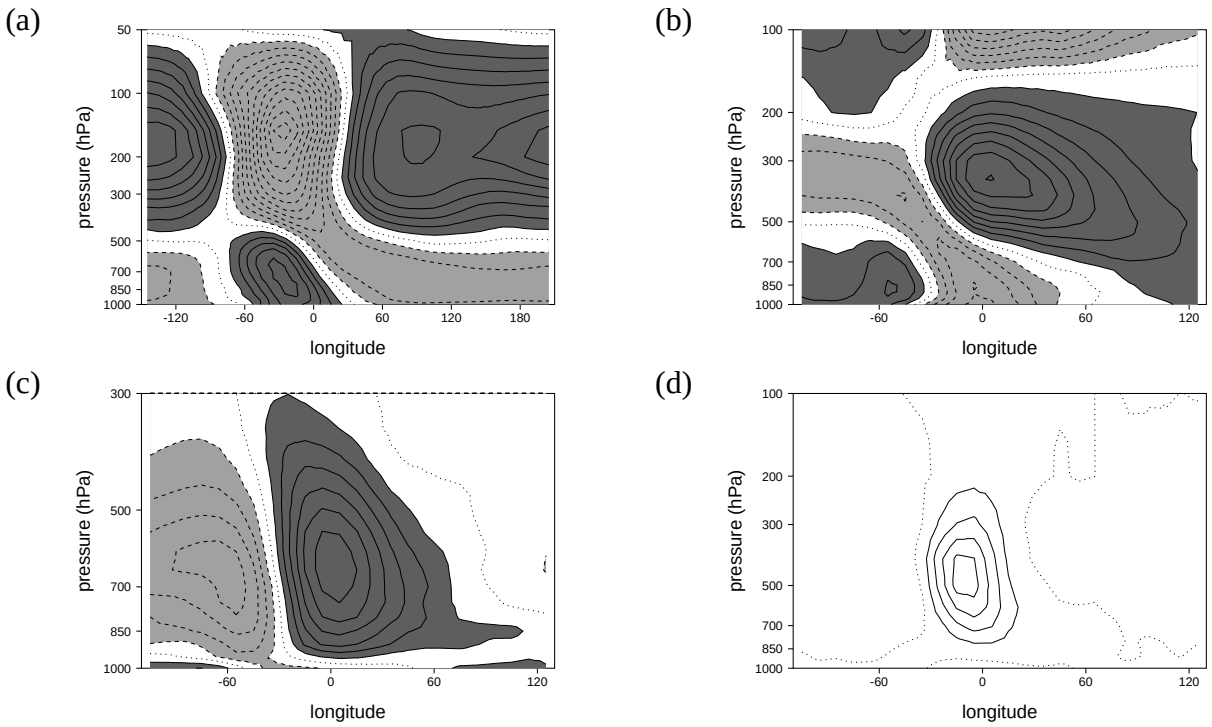

Figure 10. Composite vertical structure of MJOs simulated with a realistic SST pattern (marked with dotted lines in Fig. 9a). (a) zonal wind perturbations (1 $m\ s^{-1}$ contour interval). (b) temperature (0.3 K contour interval). (c) specific humidity (1 g/kg contour interval). (d) heatings (1 K/day contour interval). Longitude 0 corresponds to the center of the convection.

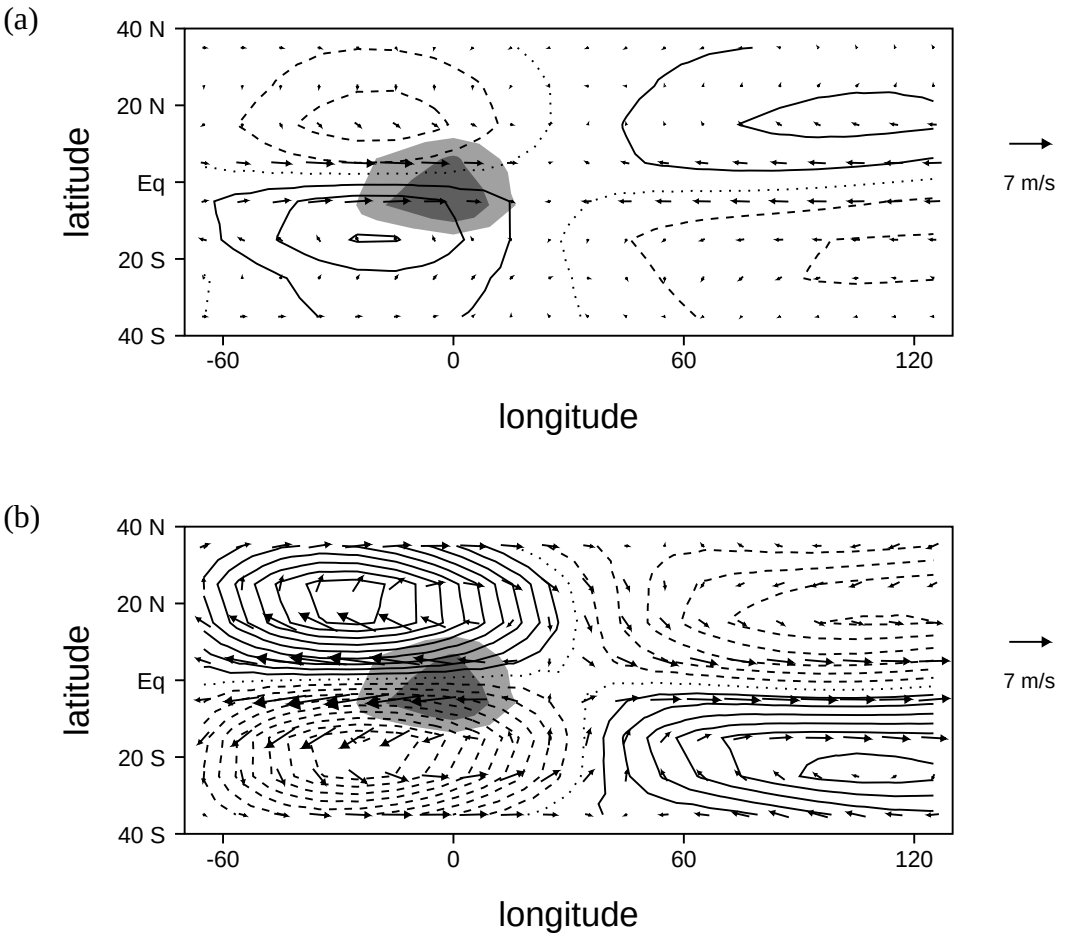

Figure 11. Horizontal structure of the composite MJO simulated with realistic SST patterns. (a) 850 hPa flow vectors and streamlines. (b) 200 hPa wind vectors and streamlines. Note the Rossby gyres to the west of the convective center in the lower troposphere and the classic quadrupole structure in upper level streamlines. Regions of rainfall exceeding 3 and 5 mm/day are shaded light and dark respectively. The contour interval for streamfunctions is $10^6 m^2 s^{-1}$.

(a)

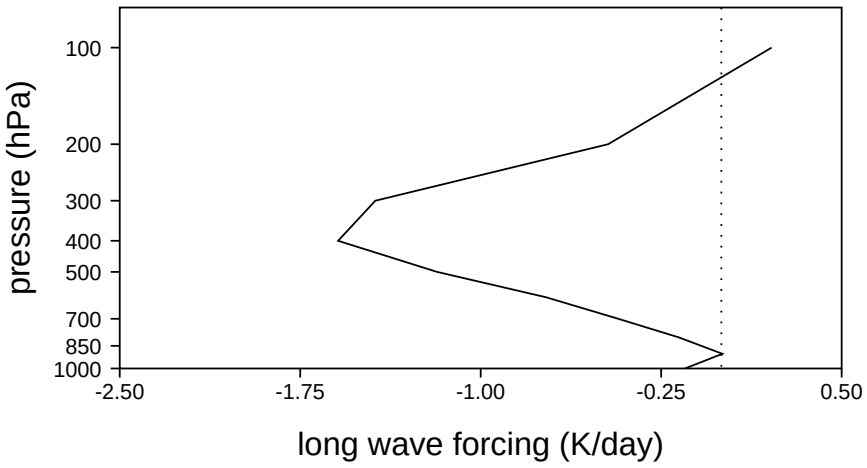

(b)

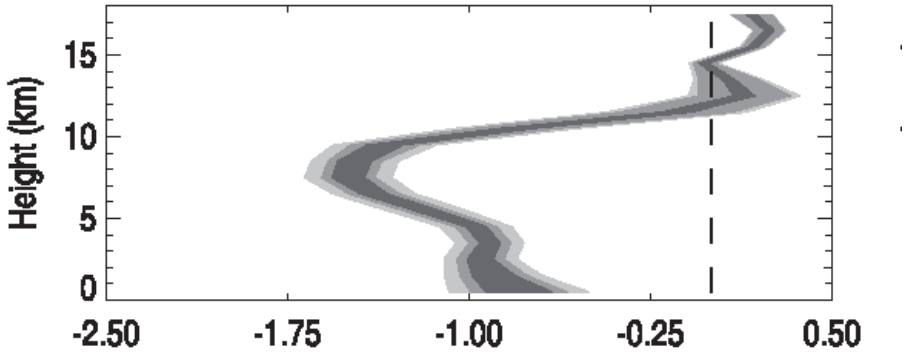

Figure 12. Vertical structure of net radiative forcing over the western Pacific warm pool in (a) LAM simulations with the new radiation scheme and (b) estimates from L'Ecuyer et al. 2010. Note that the LAM includes only longwave forcing, with a reduction in the total radiative flux to account for the lack of shortwave forcing, whereas the observed profile includes both longwave and shortwave forcing. The parameters for the radiation scheme in the LAM are tuned to make the altitude of the peak cooling and overall amplitude similar to those observed in nature.

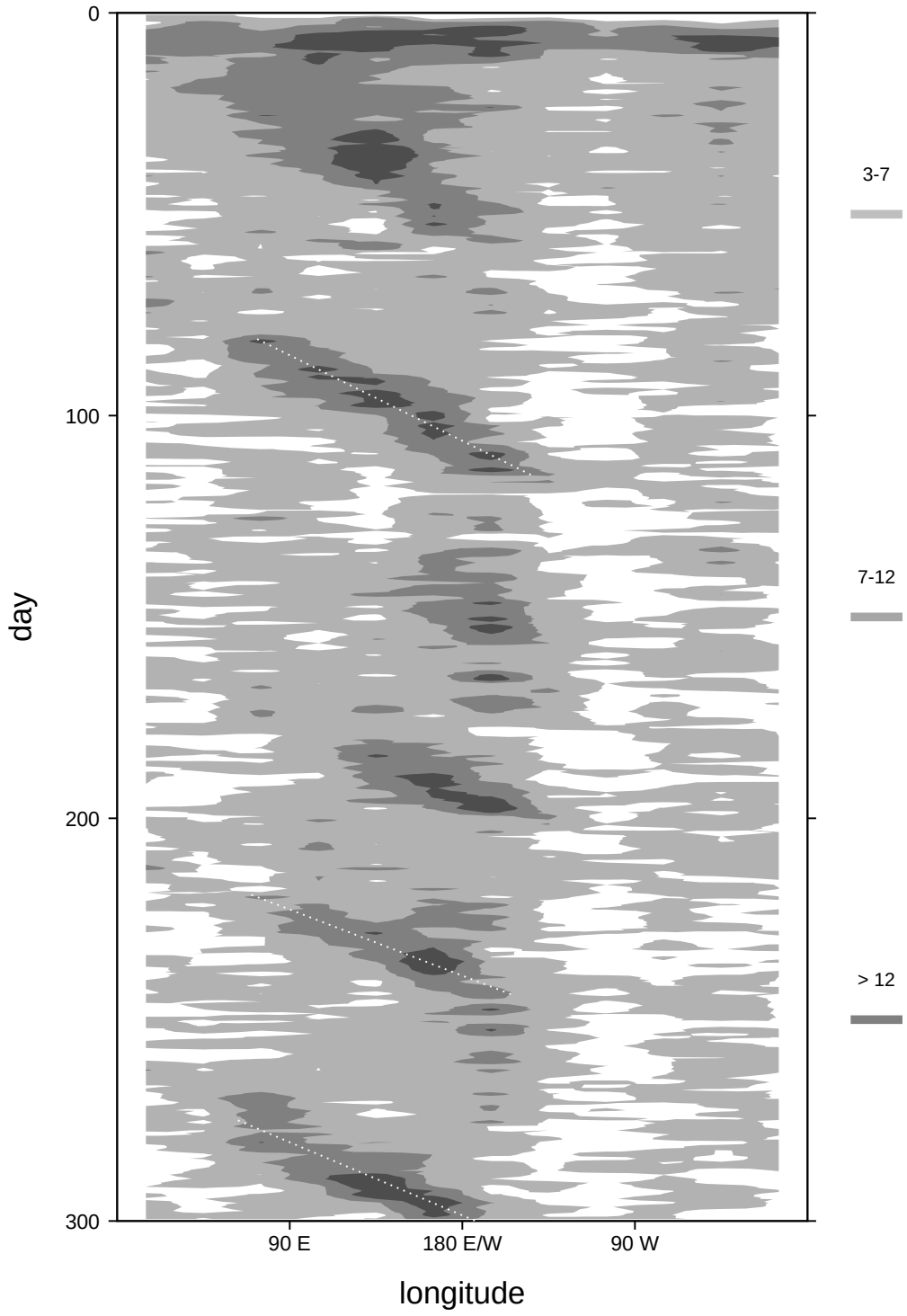

Figure 13. Time pressure series of rainfall (mm/day) for a simulation with the new radiation scheme. Approximate paths of three long lived MJOs are marked with dotted lines. Composite vertical and horizontal structures of these disturbances are shown in the following figures.

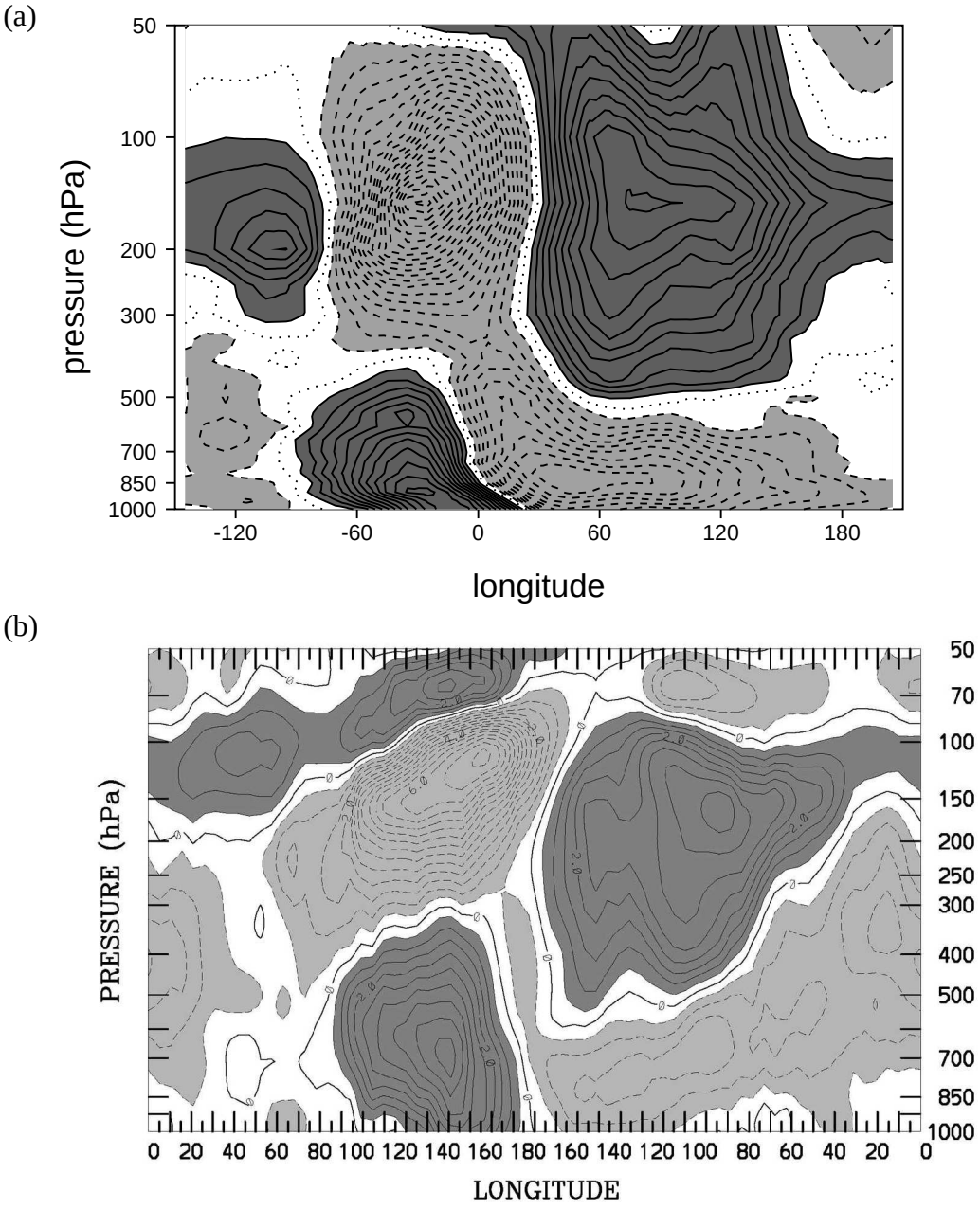

Figure 14. Composite vertical structure of zonal wind (0.5 $m\ s^{-1}$ contour interval) for (a) simulated and (b) observed MJOs. The observed structure is taken from Kiladis et al. (2005).

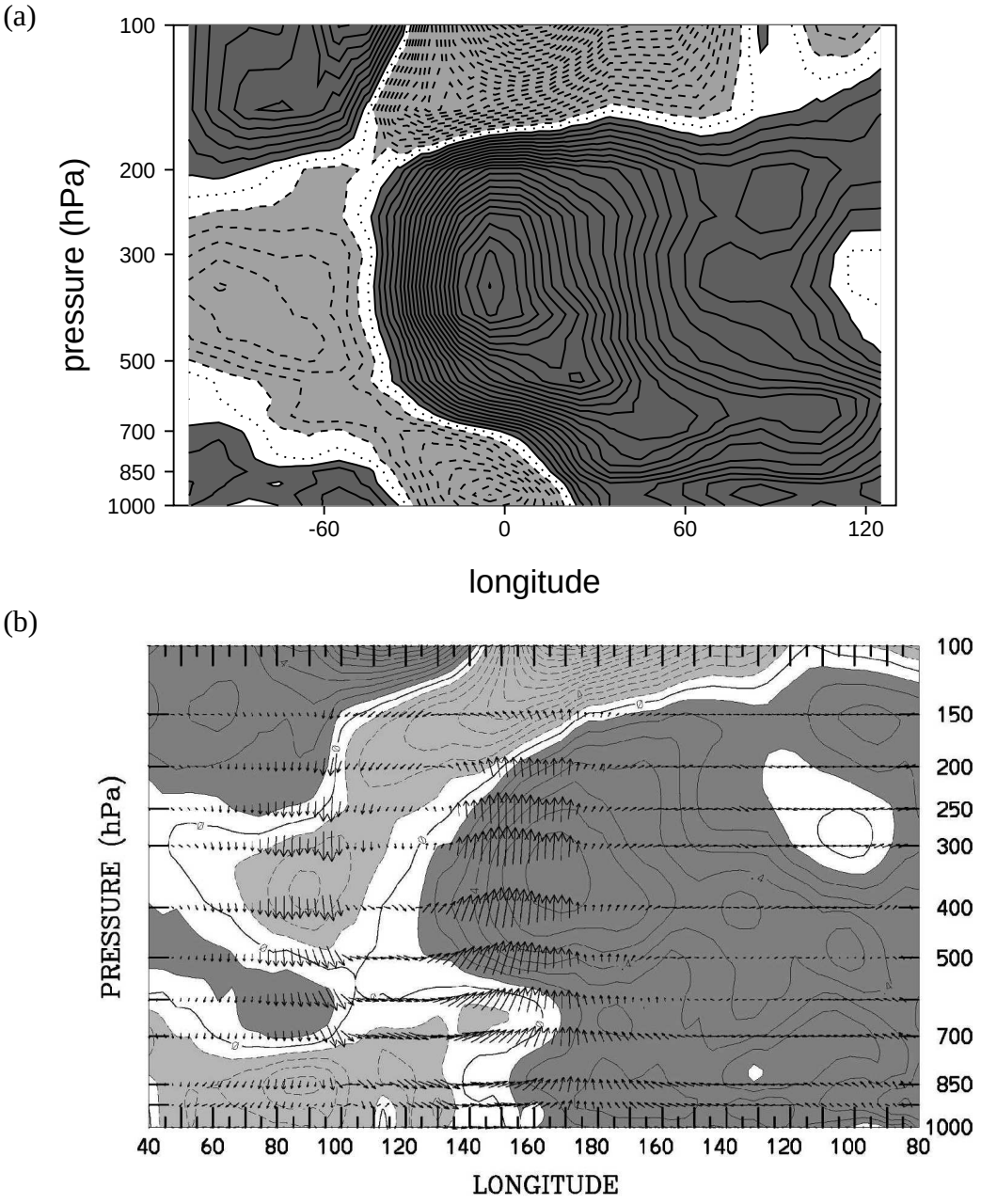

Figure 15. Composite vertical structure of temperature (0.1 *K* contour interval) for (a) simulated and (b) observed MJOs. The observed structure is taken from Kiladis et al. (2005).

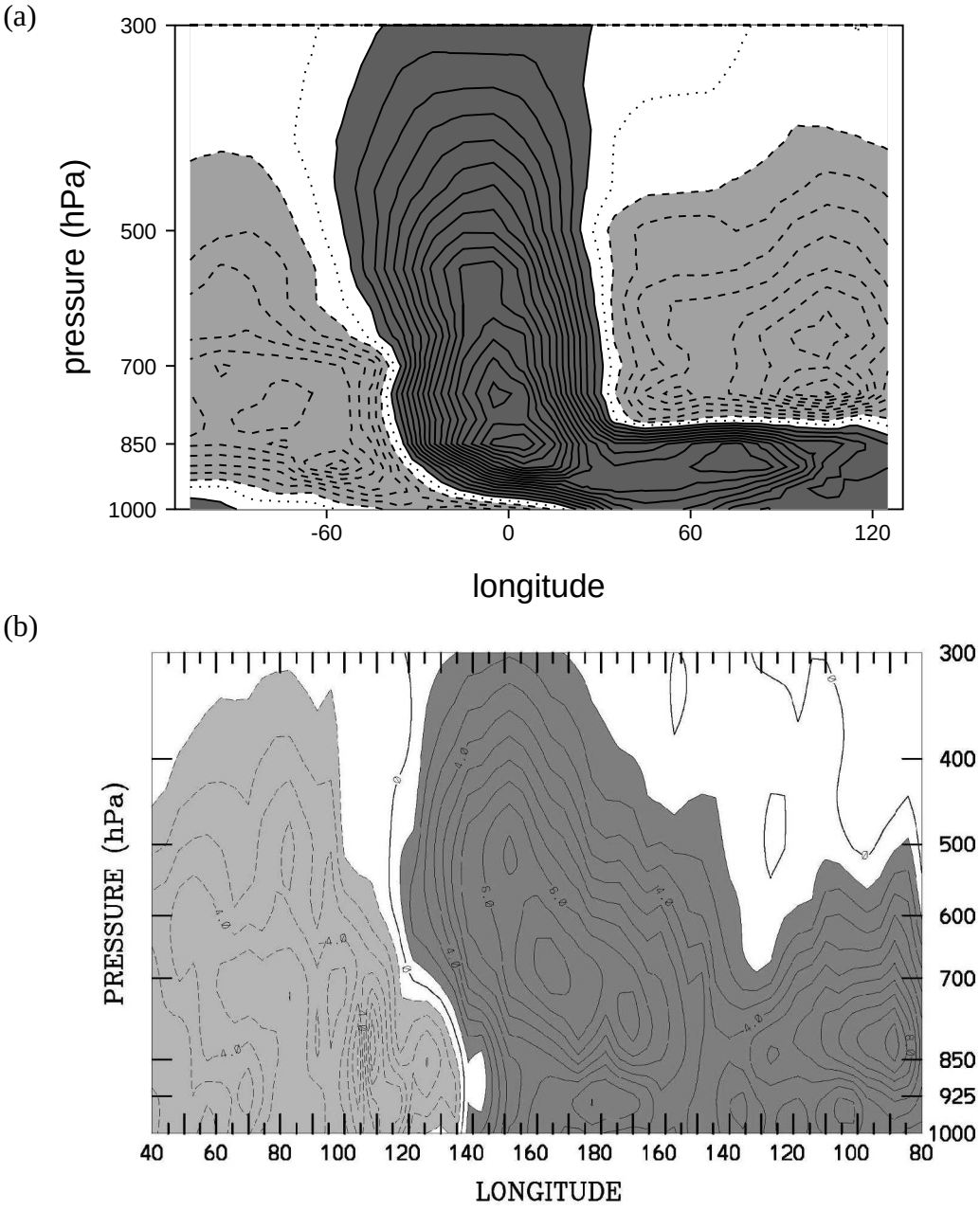

Figure 16. Composite vertical structure of specific humidity (0.1 $g\ kg^{-1}$ contour interval) for (a) simulated and (b) observed MJOs. The observed structure is taken from Kiladis et al. (2005).

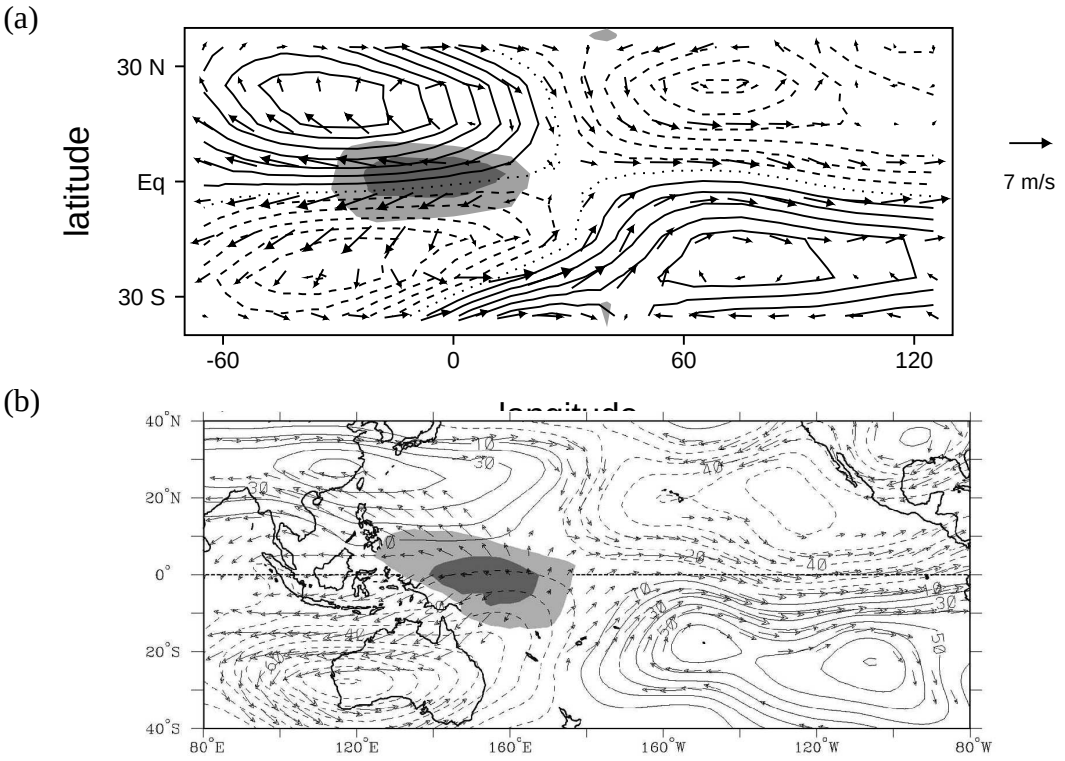

Figure 17. Composite horizontal structures of 200 hPa flow ($10^6 m^2 s^{-1}$ contour interval) for (a) simulated and (b) observed MJOs. The observed structure is taken from Kiladis et al. (2005). Regions of precipitation with values greater that 3 and 7 $mm\ day^{-1}$ are shaded light and dark in panel (a) respectively. Outgoing longwave perturbations of less than -16 and -32 $W\ m^{-2}$ are shaded light and dark in panel (b) respectively.

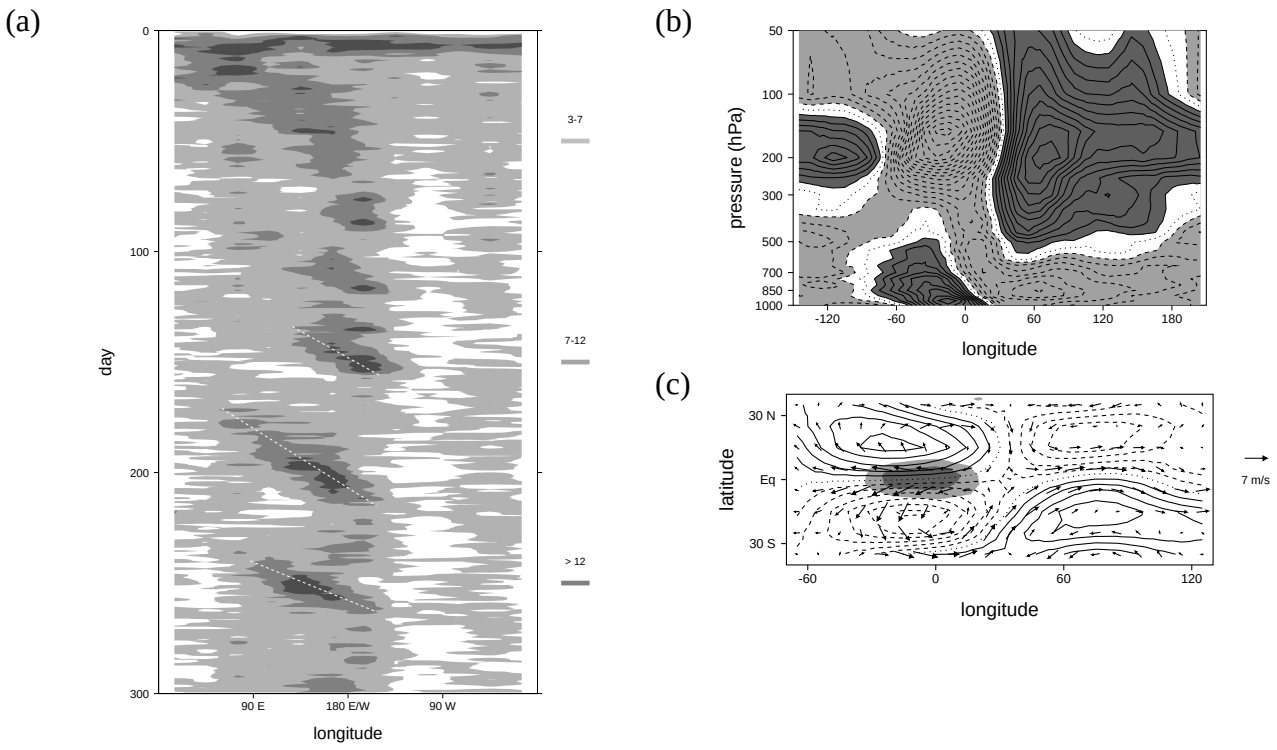

Figure 18. Simulations of MJOs using a moisture independent or "gray" radiative transfer equation. (a) time pressure series of rainrate (mm/day). (b) composite MJO zonal wind structure. (c) composite MJO 200 hPa flow. Note that MJO amplitude and structure is similar to that generated with the moisture dependent radiative transfer scheme (Figs. 13, 14a, 17a).

(a)

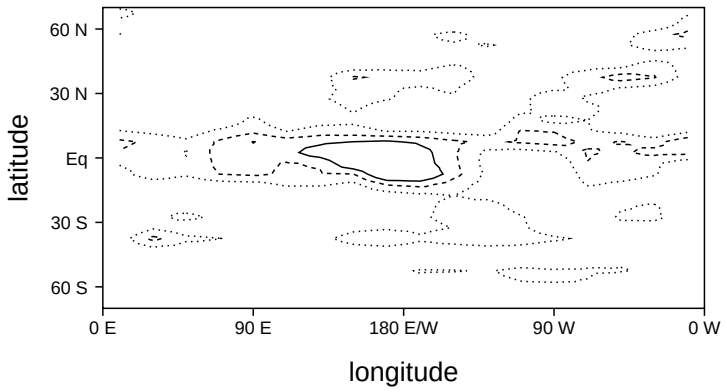

(b)

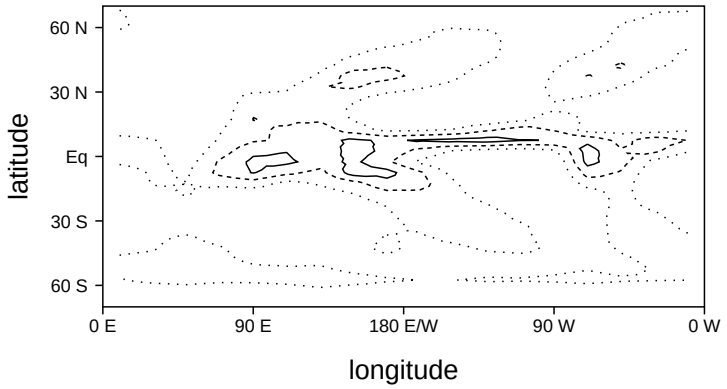

(c)

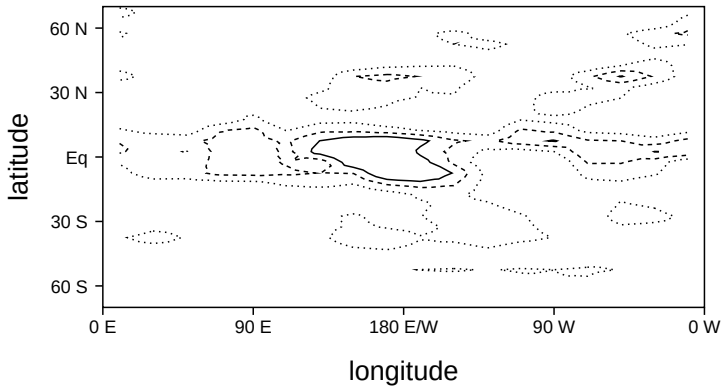

Figure 19. Relationship between precipitation patterns and MJO activity. (a) Time average precipitation (3, 5, 7 mm/day contours are dotted, dashed, solid lines respectively) for the LAM simulation with an active MJO depicted in Figs. 13-17. (b) Observed annual rainfall from the GPCP data set for 1979-2010. (c) time average precipitation from a LAM simulation with reduced evaporation.

(a)

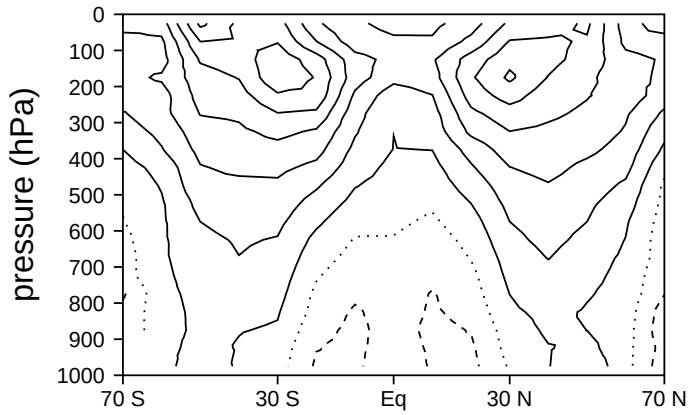

(b)

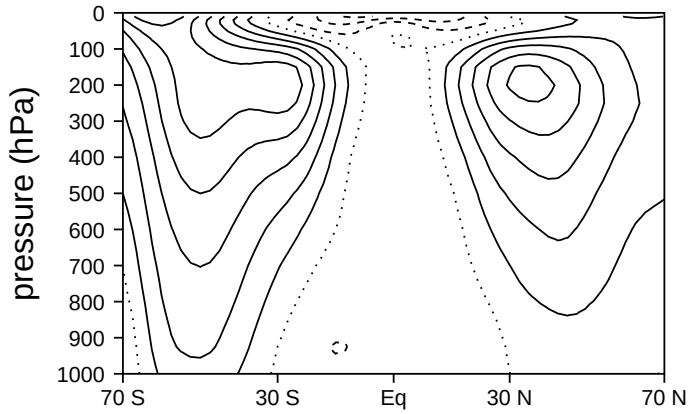

(c)

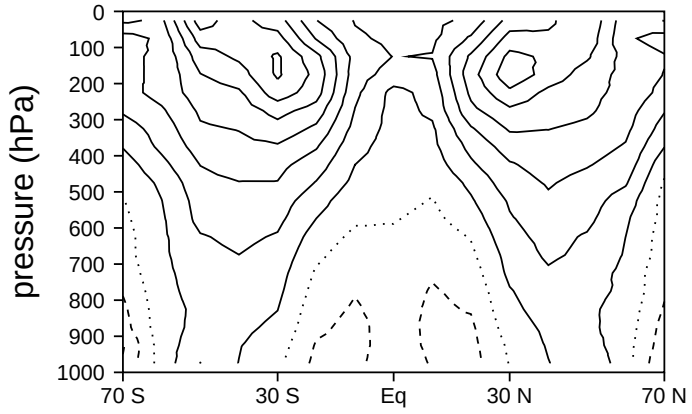

Figure 20. Zonal average zonal wind (5 $m\ s^{-1}$ contour interval). (a) LAM simulation with MJO favorable model parameters. (b) Observed (NCEP-DOE Reanalysis 2 for the period 1979-2010). (c) LAM simulation with reduced entrainment/detrainment. LAM zonal wind averages are calculated by dividing the meridional domain into 10^{o} wide sections and averaging zonal velocities of parcels centered in each section.

(a)

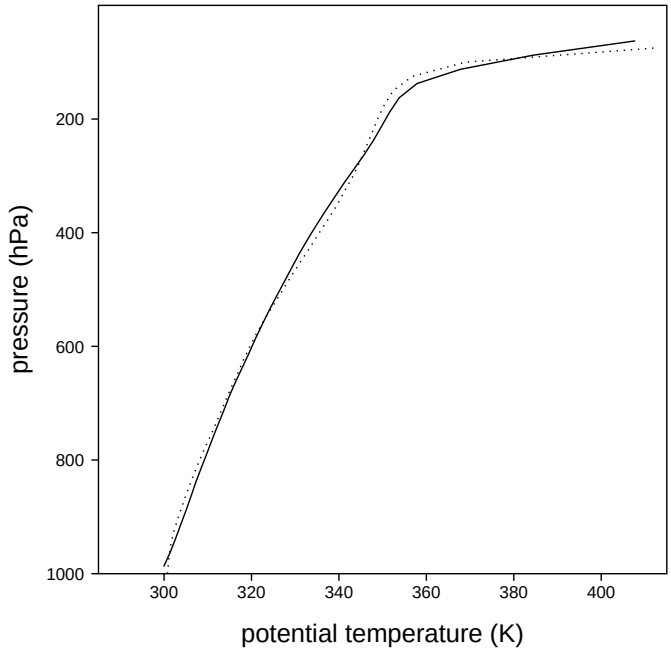

(b)

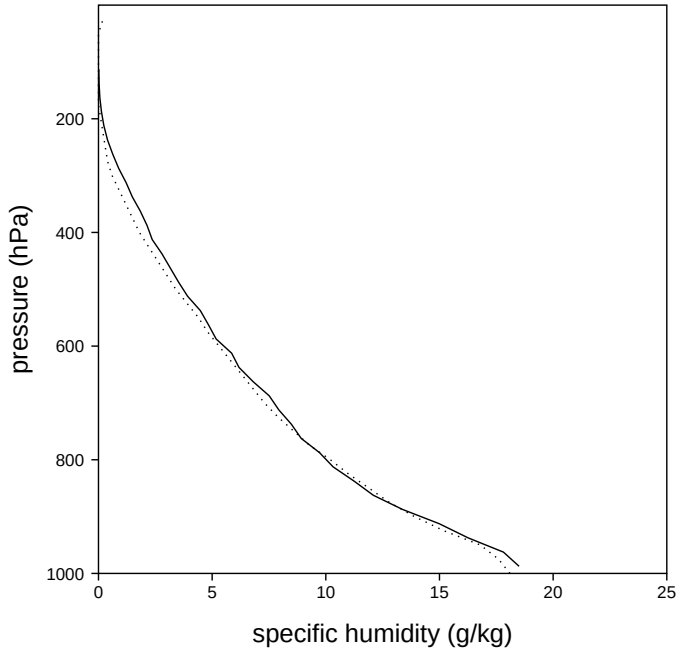

Figure 21. Vertical profiles of temperature and moisture over the western Pacific warm pool for the simulation with a reduced entrainment/detrainment parameter and a weaker MJO (to be compared with Fig. 3).

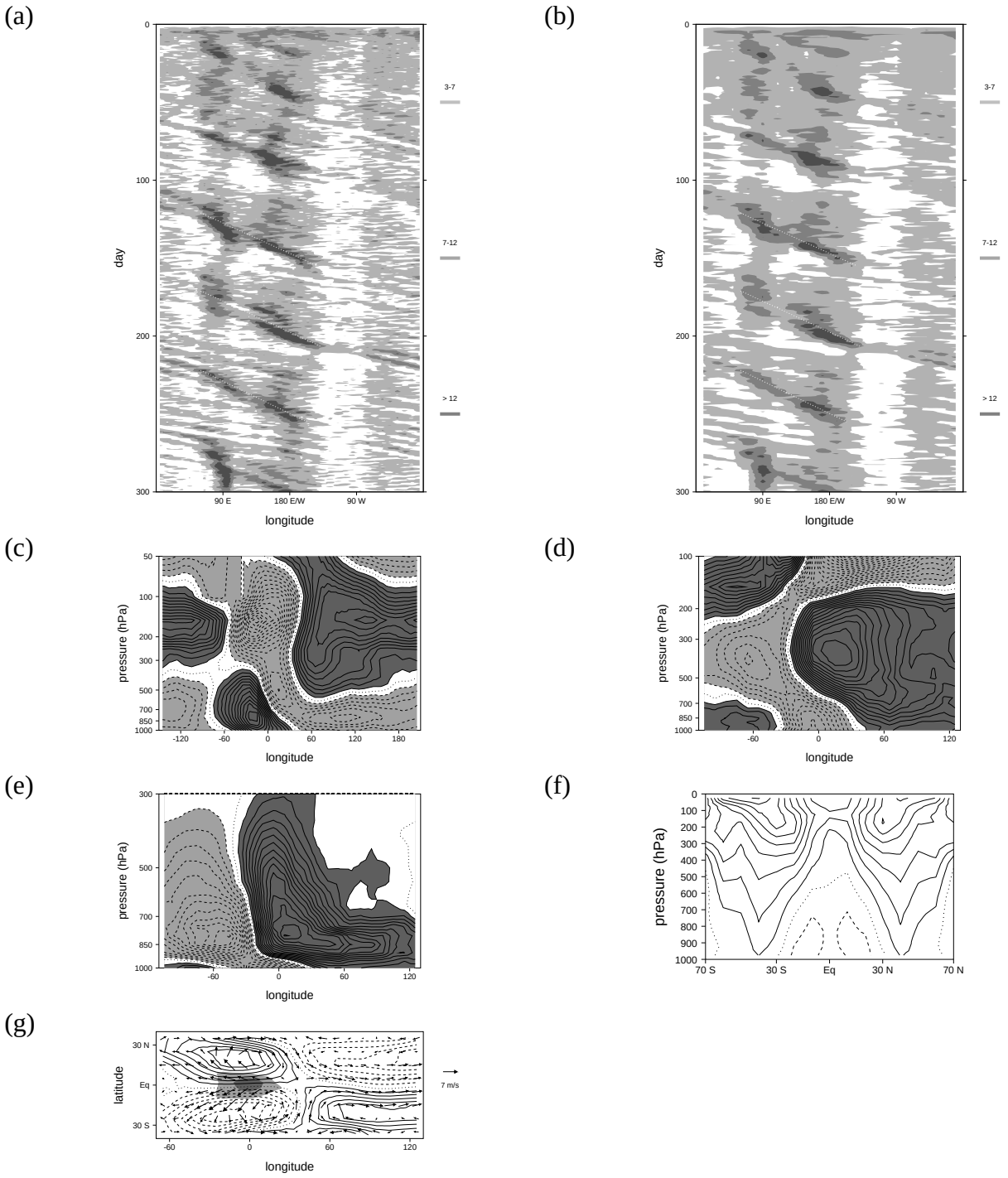

Figure A1. Results of a higher resolution sensitivity test. (a) time pressure series of rainfall showing a series of MJOs with embedded Kelvin waves and 2-day waves. (b) time pressure series of rainfall spatially and temporally smoothed to elucidate gross MJO structure (compare with Fig. 13). (c) composite MJO perturbation zonal wind (0.5 $m\ s^{-1}$ contour interval). (d) composite MJO perturbation temperature (0.1 K contour interval). (e) composite MJO perturbation specific humidity (0.1 $g\ kg^{-1}$ contour interval). (f) zonal average zonal wind (5 $m\ s^{-1}$ contour interval) (g) composite MJO 200 hPa flow ($10^6 m^{\ 2} s^{-1}$ contour interval).

Table 1: Model parameters for idealized MJO simulations

LO column width	SF	mixing	evaporation	radiative cooling
30^o, 12^o	1,3,7,12	$17 \times 10^{-6} Pa^{-1}$	0.03	0.7 $K\ day^{-1}$

Table 2: Model parameters for radiation sensitivity tests

run	LO column width	SF	mixing	evaporation
control	20^o, 5^o	7	$40 \times 10^{-6} Pa^{-1}$	0.05
reduced evaporation	20^o, 5^o	7	$40 \times 10^{-6} Pa^{-1}$	0.03
reduced mixing	20^o, 5^o	7	$30 \times 10^{-6} Pa^{-1}$	0.05

Table 3: Model parameters for resolution sensitivity test

LO column width	SF	mixing	evaporation
10^o, 2.5^o	7	$40 \times 10^{-6} Pa^{-1}$	0.07